Carrier-mediated control over the soft mode and ferroelectricity in $BaTiO_3$

Fangyuan Gu, Éamonn Murray, and Paul Tangney
Department of Physics and Department of Materials,
Imperial College London, London SW7 2AZ, UK
(Dated: February 5, 2021)

We calculate the effects of conduction band electrons (CBEs), introduced by doping or photoexcitation, on the ferroelectricity and phonon dynamics of $BaTiO_3$ (BTO). We show that CBEs destabilize ferroelectricity, which would lower the Curie temperature and coercive field, and might help to improve the speed or efficiency with which polarization domains can be switched in ferroelectric devices. We show that CBEs lower the frequencies of the A_1 soft/ferroelectric modes in BTO's ferroelectric phases, and raise the soft mode frequency in its paraelectric phase. We also show that femtosecond laser pulses could be used to *selectively* excite a coherent A_1 ferroelectric-mode phonon. This would allow this much-studied excitation to be monitored by pump-probe spectroscopy as it decays into other modes. We show that many of the properties of doped and undoped BTO have simple and intuitive explanations, within an ionic picture of BTO's bonding, if it is assumed that ferroelectricity is not driven by long range interactions, but by the attraction between Ti and O neighbours. Most of the effects of CBEs are consequences of them reducing ions' charges and increasing their polarizabilities, thereby weakening the Ti-O attraction. As the CBE density increases, so does the density of delocalized interstitial electrons, which would increase conductivity. We argue that a polar metallic phase exists if the threshold for metallic conductivity can be reached before the CBEs make polar distortions energetically unfavourable by critically weakening the Ti-O attraction.

I. INTRODUCTION

$BaTiO_3$ (BTO) is a high-κ ceramic that is ferroelectric, ferroelastic, piezoelectric, and pyroelectric. Among ABO_3 perovskites materials, it is often viewed as the simplest multiferroic and the archetype of ferroelastoelectrics - an important class of functional materials. Therefore, it is of both fundamental and practical importance to understand BTO's structure, energetics, phonon dynamics, and the intimate relationship between its ferroelectric and ferroelastic orderings.

BTO is used in many devices, including capacitors, tunable microwave devices [1], transducers, and sensors [2, 3]. It is also being studied for its potential use in ferroelectric memory devices (FeRAM), photovoltaic devices [4–9], for electro-optic modulation [10] and for energy storage [11–14]. It is often doped or alloyed with other perovskite materials, such as $SrTiO_3$, to achieve optimal properties for device applications. For example, although the optical gap (E_g) of pure BTO is around 3.2 eV [15, 16, 112], doping it with electrons (e^-) can make it semiconducting or metallic. Several experimental groups have even reported the existence of a polar metallic phase in n-doped BTO [17–19]. This coexistence of ferroelectricity and metallic conductivity is an exciting and fundamentally-important finding, which may lead to new applications. However, it is controversial [20] and not yet well-understood. Although different experimental reports of this phase are in broad qualitative agreement, the agreement is not fully quantitative. Furthermore, some of the reported measurements and spectra have not satisfactorily been explained. This is not surprising given that, after 70 years of experimental, theoretical, and computational investigations, large gaps in our understanding of *pure* (insulating) BTO remain.

At temperatures (T) greater than the Curie temperature, $T_C \approx 120^\circ\,\mathrm{C} - 130^\circ\,\mathrm{C}$, BTO is paraelectric (PE) and its nominal structure is that of a perfectly-cubic perovskite. As T is reduced, it undergoes the following sequence of phase transitions: cubic ($Pm\bar{3}m$) $\xrightarrow{393\,\mathrm{K}}$ tetragonal ($P4mm$) $\xrightarrow{278\,\mathrm{K}}$ orthorhombic ($Amm2$) $\xrightarrow{183\,\mathrm{K}}$ rhombohedral ($R3m$), where the three lower-T phases are all ferroelectric (FE) and ferroelastic. The mechanisms of the T-induced phase transitions [21, 22], and the related question of how closely the microscopic structures of these four phases match the space- and/or time-averaged structures observed experimentally [23–25], is still being debated after decades of research [26–29]. This lack of clarity or consensus can be attributed, in part, to the fact that multiple strongly-coupled modes of lattice vibration play important roles in the phase transitions, not all of which can accurately, or perhaps even usefully, be described by phonon theory. Analyses of experimental Raman and THz spectra are frustrated by this clutter, by the complexity of the interactions between the modes, and by the existence, near T_C, of a broad and strongly T-dependent spectral feature, known as the *central mode* (CM), which spans a wide range of low frequencies ($\sim 0\,\mathrm{THz} - 3\,\mathrm{THz}$). It is almost certainly not coincidental that the CM partially obscures the frequency range of most relevance to ferroelectric-ferroelastic coupling and to the acousto-optical couplings that mediate the phase transitions.

In this work we use a constrained form of density functional theory (DFT) to calculate the effects on BTO's structure, energetics, phonon dynamics and ferroelectricity of altering its electronic state by populating its conduction band with electrons. We explain the results of our calculations using a simple and intuitive ionic picture of BTO's bonding and electronic structure.

One of our purposes is to show that above-band-gap ($>E_g$) ultrashort ($\lesssim 100$ fs) laser pulses would selectively excite a coherent long-wavelength ($\mathbf{\Gamma}-$point) *soft mode* (SM) phonon in BTO's FE phases, and temporarily lower T_C and the magnitude of the coercive field (E_c) required to switch the direction of its polarization ($\mathbf{P}$). It is generally accepted that understanding the SM is crucial to understanding BTO's phase transitions [30, 31]. Therefore it seems likely that much more could be learned about it, and its relationships to other modes, by selectively exciting it at low T and monitoring its decay. We suggest that this could be achieved by ultrafast pump-probe spectroscopy with $>E_g$ pump pulses. Furthermore, interest in the use of laser pulses to help manipulate $\mathbf{P}$ domains in FE devices [5, 32] has surged in recent years. Various mechanisms have been reported, including localized heating of the lattice [33], coupling of $<E_g$ pulses to charged domain walls [34–38]; coupling of THz pulses to the SM phonon [39, 40]; indirect excitation of the SM phonon by resonant infrared (IR) excitation of a mode that couples strongly to it [41, 42]; and by impulsive stimulated Raman scattering [33, 43]. We demonstrate a non-thermal mechanism by which laser pulses could facilitate domain switching in pure or $n-$doped BTO by lowering E_c.

Our other purpose is to help explain the results of recent experiments on electron doped BTO. The simple picture of ionic bonding with which we interpret our calculations can also explain some of the puzzling properties that have been observed, including the non-monotonic dependence of the SM frequency (ν_{SM}) on carrier density [18, 44], the enhanced SM spectral intensity and weakened polarization anisotropy of the polar metallic phase[18], and the coexistence of polar distortions and metallic conductivity.

A. A_1 phonon modes and the ferroelectric instability

The FE structures of BTO can all be viewed as the result of slight symmetry-lowering distortions of the cubic PE crystal, which are driven by the attraction between Ti cations (nominally Ti^{4+}) and O anions (nominally O^{2-}). This attraction draws neighbouring Ti and O ions closer, thereby displacing them from their high-symmetry positions at the center of the conventional cubic perovskite cell and at the centers of its faces, respectively (see Fig. 1). This lowers the Coulomb energy, polarizes the crystal and, as a demand of the lowered symmetry, strains the unit cell. In all cases the resulting $\mathbf{P}$ is parallel to the (average) off-center Ti displacement.

The equilibrium polar distortions are not unique: for example, in the R3m phase Ti can be displaced in the direction of any one of the eight Ba atoms at the cell's corners, i.e., along any $\langle 111\rangle$ direction. Its ferroelectricity can be attributed, firstly, to the existence of these multiple energy minima, corresponding to different polarizations, and, secondly, to the shallowness of these minima, which allows $\mathbf{P}$ to be switched by an applied field.

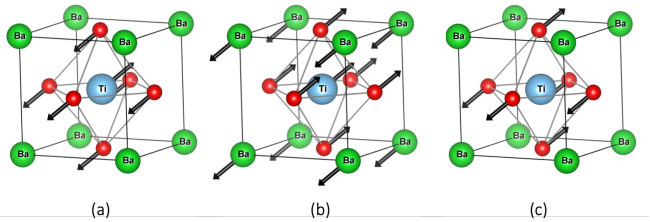

FIG. 1. Eigen-displacements of $BaTiO_3$ zone-centre (a) Soft mode (SM), (b) Last mode (LM) and (c) Axe mode (AM) in rhombohedral phase. Green, blue and red balls mark Ba ions, Ti ions and oxygens, respectively.

The space groups of the FE phases are all subgroups of $Pm\bar{3}m$ and, as a consequence of their lowered symmetry, each FE phase possesses A_1 phonon modes. A_1 modes preserve symmetry in the sense that a small perturbation of a crystal along an A_1 eigenvector does not lower or raise the crystal's symmetry. Furthermore, the parent high-symmetry $Pm\bar{3}m$ structure can be reached from each FE crystal by a linear combination of displacements along the latter's A_1 eigenvectors. Therefore the ferroelectric instability can be viewed as an instability of $Pm\bar{3}m$ to distortion along the FE phases' A_1 eigenvectors. The $Pm\bar{3}m$ crystal does not possess A_1 modes because all atoms in its unit cell occupy positions of high symmetry and so any small perturbation would lower the crystal's symmetry. Each FE phase has three polar A_1 modes, which are both IR- and Raman-active, and whose eigenvectors are illustrated in Fig. 1. The SM is one of these; it involves the counter-motion of the Ti ion and the octahedral 'cage' whose vertices are the six nearest O ions to it. The eigendisplacements of the other two IR- and Raman-active A_1 modes can roughly be described as motion of rigid TiO_6 octahedra relative to the Ba sublattice ("*Last mode*", LM), and a rotation and deformation of the O_6 octahedral cage within stationary cation sublattices ("*Axe mode*", AM).

The fact that A_1 eigenvectors relate a FE phase to the PE phase is crucial. It means that the magnitude of the polar distortion of the $Pm\bar{3}m$ structure, and hence $|\mathbf{P}|$, is not constrained by symmetry but determined by competition between the Ti-O Coulomb attraction and the 'exchange' repulsion between the ions' overlapping electron clouds [45]. It follows that any means of altering the delicate balance between these opposing forces can be used to control ferroelectricity and ferroelasticity. One practical way to effect such a change, which is the subject of the present work, is to populate the conduction band (CB) with electrons.

B. Soft mode, ferroelectric mode, central mode

Much of the work towards understanding the phase transitions in BTO has focussed on the SM [22], which is a triply-degenerate IR-active and Raman-active transverse optical (TO) F_{1u} phonon that softens incompletely as T_C is approached from above [46], and which splits, at the PE-FE transition, into a dramatically-hardened A_1 mode and two degenerate E modes. The E modes continue to soften until one of them hardens at each of the FE-FE phase transitions. In FE phases the A_1 counterpart of the SM is known as the *ferroelectric mode* (FM) because the countermotion of Ti and its O cage is along the polar axis and, in the long-wavelength limit, the FM is simply an oscillation of $\mathbf{P}$.

The CM mentioned in the introduction is a further IR- and Raman-active mode, which is observed in both FE and PE phases [30, 47]. It is thought to be thermally-activated and to be overdamped, or heavily damped if/when it is oscillatory [22]. A plausible explanation of it has been provided by Hlinka *et al.* [48]. What follows is a brief summary of their explanation as it would apply to a simplistic model of ferroelectricity in BTO.

We notionally partition the crystal into primitive unit cells and let $\mathbf{d}$ denote the difference between a particular cell's instantaneous dipole moment and the dipole moment it would have in the perfect $Pm\bar{3}m$ crystal. The latter is zero for some choices of unit cell. The macroscopic polarization is $\mathbf{P} = \langle\, \mathbf{d} \,\rangle \,/\, \langle\, \Omega \,\rangle$, where Ω denotes a primitive cell's volume and $\langle\ \rangle$ denotes an average over different cells (space) or time. We refer to the fluctuation of $\mathbf{d}$ within a cell as one of the crystal's *local modes* and, for simplicity, we assume that it is dominated by the contribution to it from distortion of the $Pm\bar{3}m$ primitive cell along the FE phase's $\mathbf{\Gamma}$-point A_1 FM eigenvector. In R3m $\mathbf{d}$ arises from a distortion of $Pm\bar{3}m$ along the eigenvector illustrated in Fig. 1(a). In P4mm and Amm2 it arises from counter-motion of Ti and its O_6 cage along the $\langle 100 \rangle$ and $\langle 110 \rangle$ directions, respectively. We now consider the coupled dynamics of the $\mathbf{d}$'s and we focus specifically on their components parallel to $\mathbf{P}$, which we denote by d.

We approximate the FM+CM part of each cell's energy as $\mathcal{E}^{\mathrm{FM+CM}} = \mathcal{E}^{\mathrm{FM+CM}}_{\mathrm{local}} + \mathcal{E}^{\mathrm{FM+CM}}_{\mathbf{d}-\mathbf{d}}$, where $\mathcal{E}^{\mathrm{FM+CM}}_{\mathbf{d}-\mathbf{d}}$ is the coupling to $\mathbf{d}$'s in other cells and $\mathcal{E}^{\mathrm{FM+CM}}_{\mathrm{local}}(d)$ is independent of other cells. By symmetry $\mathcal{E}^{\mathrm{FM+CM}}_{\mathrm{local}}(d) = \mathcal{E}^{\mathrm{FM+CM}}_{\mathrm{local}}(-d)$; therefore, if we also assume *weak coupling* between cells, i.e., $\left|\mathcal{E}^{\mathrm{FM+CM}}_{\mathbf{d}-\mathbf{d}}\right| \ll \left|\mathcal{E}^{\mathrm{FM+CM}}_{\mathrm{local}}\right|$, we find that $\mathcal{E}^{\mathrm{FM+CM}}(d)$ is an almost-symmetric double well potential. $\mathcal{E}^{\mathrm{FM+CM}}_{\mathbf{d}-\mathbf{d}}$ is responsible for the slight asymmetry that favours the $d > 0$ ($\Rightarrow \mathbf{d} \parallel \mathbf{P}$) energy basin over the $d < 0$ ($\Rightarrow \mathbf{d} \parallel -\mathbf{P}$) basin. At low T each $d(t)$ oscillates near its $d > 0$ energy minimum with amplitude $\propto \sqrt{T}$ and a probability $\propto \exp\left(-\Delta\mathcal{E}^{\mathrm{FM+CM}}/k_B T\right)$ of *hopping* to the $d < 0$ basin, where $\Delta\mathcal{E}^{\mathrm{FM+CM}}$ is the barrier separating the two basins. At finite T some fraction of the d's are negative, which reduces $|\mathbf{P}|$, thereby lessening the asymmetry of $\mathcal{E}^{\mathrm{FM+CM}}(d)$. When T is low enough we can understand the FM and the CM as different forms of collective motion of all the d's in the crystal: the FM is coupled small oscillations of the d's about one of their two local energy minima and the CM is their coupled low-frequency hopping between the two energy basins. The fact that each d has more than one local minimum adds considerable complexity to the FM, which we do not discuss here. The FM and CM coexist, but as T increases and hopping becomes more frequent the CM steals more of the FM's spectral intensity. At high T the assumption of weak coupling breaks down and, effectively, each d moves on a time-dependent potential energy surface (PES), $\mathcal{E}^{\mathrm{FM+CM}}(d,t)$, whose instantaneous shape is determined by the structures of surrounding cells [49]. Above T_C, thermal disorder among the d's ensures symmetry, on average, of each local PES, $\mathcal{E}^{\mathrm{FM+CM}}(d)$, about $d = 0$, so that $\langle\, \mathbf{d} \,\rangle = \mathbf{P} = 0$.

If the coupling between local modes remained weak as T increased, the hopping probability would approach one and each d would oscillate freely between positive and negative values. Even if the local PES still had a double well when the d's were disordered, its features would appear flat on the scale of $k_B T$. The FM would have vanished, giving up all of its spectral intensity to the CM, which now consists of coupled oscillations of the d's about zero. As T increases above T_C the frequency of the CM, ν_{CM}, would increasingly be determined by the side walls of $\mathcal{E}^{\mathrm{FM+CM}}(d)$, rather than by its almost-flat base (near $d = 0$), where each local mode spends a diminishing fraction of its time.

Because the CM involves local modes traversing the energy barriers separating their two local energy minima, phonon theory, which relies on potential energy being well approximated by a low-order Taylor expansion about a single energy minimum, cannot be relied on to provide an accurate, or even useful, description of it. Essentially, the CM is a *rattler mode* [50] at low T, which means that the distribution of its energy in $(\omega, \mathbf{k})-$space is diffuse and overlaps with many acoustic and optical phonons, allowing it to couple to them. In phonon theory, by contrast, each mode is assumed to approximate a Dirac $\delta-$function in $(\omega, \mathbf{k})-$space.

In summary, below T_C the CM spectral intensity increases with T at the expense of the FM, and spans a wide range of low frequencies ($\lesssim 3$ THz). Above T_C, the CM and the SM are different aspects of the same anharmonic motion. To fit experimental spectra, this motion is often modelled as a damped oscillator, identified as the FM, coupled to an overdamped oscillator, which is identified as the CM [18, 48]. The purpose of this simplistic account of the FM/CM dynamics is to explain, briefly, why these modes are so important for understanding BTO's phase transitions and to lay groundwork that will help us to explain the effects of doping and photoexcitation on them.

The modes described here and in Sec. I A are ordered

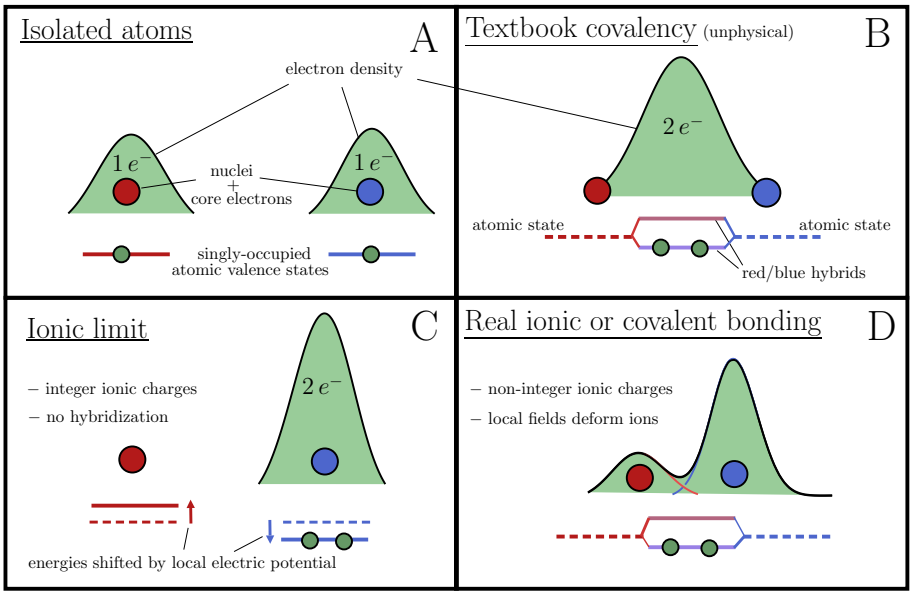

FIG. 2. Schematic. Panel A depicts the valence electron density $n(\mathbf{r})$ for two isolated (noninteracting) monovalent atoms. Panel B shows how textbooks sometimes explain covalency: electrons from each atom combine to form a packet of density along the bond; the attraction of their nuclei to this packet binds the atoms together. This picture is unphysical because the density can only be localized around maxima of the electric potential, $\Phi(\mathbf{r})$, which occur only at the nuclei. Panel C depicts the ionic limit if state hybridization is forbidden. One atom donates its valence electron to the other atom's singly-occupied valence state. The electron donor and acceptor become a cation and an anion, respectively, with charges of magnitude $1\,e$. The potential from the cation lowers the energy of the doubly-occupied valence state on the anion. In reality, states always hybridize to some degree and if ions did not overlap there would be no repulsion to balance the cation-anion attraction. Panel D depicts a more realistic ionic or covalent bond. The only density maxima are at nuclei. Ions' charges cannot be integers because the valence state is hybridized. The distribution of an ion's core electrons tends to be almost spherically symmetric because of their strong attraction to the nucleus. Valence electrons in the overlap region break radial symmetry because they feel comparable attractions to multiple nuclei. If the overlap is not too great, the material's structure and energetics are well approximated by those of a set of slightly-overlapping polarizable ions [49, 56–61].

by frequency as follows: $\nu_{\mathrm{CM}} < \nu_{\mathrm{LM}} < \nu_{\mathrm{SM,FM}} < \nu_{\mathrm{AM}}$.

C. Bonding and energetics in simple terms

Ferroelectricity in BTO is often attributed to two factors: long-range electrostatic forces are said to drive the symmetry-lowering polar distortions that transform the PE phase into the FE phases, while partial covalency of the Ti-O bond is said to facilitate this by weakening the repulsion between overlapping Ti and O ions [45, 51–55]. Overlap repulsion resists the PE-FE transition because polar distortions shorten Ti-O bonds.

In this section, we revisit both of these claims about BTO's bonding and energetics.

In Sec. I C 1 we point out that many definitions of 'covalent' and 'ionic' are in use and we clarify that the sense in which BTO has been shown to be covalent is not inconsistent with our finding that the PES on which its ions move is very close to the PES on which a set of slightly-overlapping polarizable ions would move. We also explain our decision to differ semantically from most recent literature on ferroelectricity in BTO by referring to this bonding as ionic.

In Sec. I C 2 we argue that the short-range attraction between Ti and O neighbours is more likely than long-range Coulomb interactions to be what drives the PE-FE transitions.

1. *Ionic or partially covalent?*

According to standard algorithms for determining oxidation states of ions [62], the electronic configurations of the ions in BTO within tight binding theory would be Ba $6s^0$, Ti $3d^0$, and O $2p^6$, with the highest occupied and the lowest unoccupied bands being composed of O 2p orbitals and Ti 3d orbitals, respectively. Therefore, within this simplistic picture, BTO's bonding conforms to the simple ionic limit depicted in Fig. 2 C, with the Ba, Ti, and O ions having integer charges of $q_{\mathrm{Ba}} = +2\,e$, $q_{\mathrm{Ti}} = +4\,e$, and $q_{\mathrm{O}} = -2\,e$, respectively, where e is the magnitude of an electron's charge. However, since the work of Cohen and Krakauer in the 1990s [45, 51], the prevailing view has been that there is a significant degree of covalency to the Ti-O bond in BTO, and that this plays an important

role in stabilizing BTO's ferroelectric phases by reducing the short range repulsion between ions.

It is important to clarify what Cohen actually found because the terms 'covalent' and 'ionic' are notoriously difficult to define and neither term has a definition that is both precise and commonly accepted [63–73]. For example, one can still find modern textbooks describing a covalent bond as it is depicted in Fig. 2 B [74–76]: one or more pairs of electrons (an even integer number) are localized *between* two ion cores (nuclei + core electrons) and the atoms are bonded by the cores' common attraction to their shared bundle of electron density. This caricature of covalency dates back to early attempts to make sense of chemical bonding, including Lewis's introduction of his suggestive dot diagrams [77, 78], and Pauling's description of the electrons in a covalent bond as "*a pair of electrons held jointly by two atoms*" [63]. However, we now know that it is unphysical because if electrons were localized along a bond the electron density, $n(\mathbf{r})$, would have a local maximum there, but it does not. A universal feature of the electronic ground states of real materials is the existence of local maxima of $n(\mathbf{r})$ at the nuclei and nowhere else. This empirical observation has a formal basis, which follows from the ground state relation $e\,\Phi(\mathbf{r}) = \delta F/\delta n(\mathbf{r})$ between the electric potential from the nuclei, $\Phi(\mathbf{r})$, and the electron density, where the universal functional $F[n]$ is the sum of the electrons' kinetic energy and their mutual Coulomb repulsion [79]. This relation implies that maxima of $n(\mathbf{r})$ are always accompanied by maxima of $\Phi(\mathbf{r})$ and, since $\Phi(\mathbf{r}) \sim \sum_i |\mathbf{r} - \mathbf{r}_i|^{-1}$ only has local maxima at the positions of nuclei ($\mathbf{r}_i$), the version of covalency depicted in Fig. 2 B is fundamentally wrong. Nowadays, most researchers recognise that ionic and covalent bonding differs only by the degree to which electrons are localized around nuclei. In ionic bonding more of the valence electron density is located at points where $\boldsymbol{\nabla} n$ is directed towards the nearest nucleus, whereas in covalent bonding more of it is at points where $\boldsymbol{\nabla} n$ is not directed towards any particular nucleus because the net electric field from the nuclei, $-\boldsymbol{\nabla}\Phi$, contains significant contributions from multiple nuclei instead of being dominated by only one.

To analyse BTO's bonding, Cohen considered the decomposition of the Kohn-Sham eigenstates [80] into linear combinations of atomic orbitals (LCAOs). He tacitly *defined* covalency as the existence of occupied (valence) states that have significant projections onto atomic orbitals belonging to *both* bonded atoms. Then he showed that BTO's upper VBs [lower CBs] are not composed purely of O 2p [Ti 3d] orbitals, but are more accurately described as hybrid states composed of O 2p [Ti 3d] orbitals admixed with Ti 3d [O 2p] orbitals [45, 51]. He also showed that the ionic charges calculated from the self-consistent charge density are much smaller in magnitude than their formal values [45]. They are non-integer multiples of e, as must be the case when a state whose density is split between two ions has integer occupancy.

Cohen's definition of covalency is a practical one and it is much more sensible and realistic than the cartoon in Fig. 2 B. It is also consistent with the literal meaning of covalence ('shared valence'). However, it is simplistic, because the LCAO method is simplistic. Formally, atomic orbitals are basis functions and nothing more, and the Hohenberg-Kohn theorems [79, 81] tell us that if covalency and ionicity are qualitatively-distinct forms of bonding, they are distinguishable from the electron density alone [79]. Cohen's definition is also so broad that it labels almost all semiconductors and insulators as covalent, including materials regarded by most as ionic. For example, Bao *et al.* [82] used DFT and wavefunction-based methods to calculate the charges of a pair of Na and Cl atoms as they are brought together from a large separation. When they first begin to interact, Na donates an electron to Cl to form ions of charge $\pm 1\,e$, thereby realizing the ionic limit schematized in Fig. 2 C. As they draw even closer, their doubly-occupied valence state continuously acquires more Na character, causing the magnitudes of the charges to decrease continuously to around $0.8\,e$ at their equilibrium separation. The density of the hybridized valence state is not localized between the ion cores. It is localized on them, but divided between them. Calculations on bulk NaCl have also shown that the valence band is a hybrid of Na s and Cl p states and that charges have magnitudes of about $\sim 0.8\,e$ [68, 83, 84]. According to Cohen's definition, NaCl is partly covalent.

From Cohen's definition of covalency we infer that his definition of a purely-ionic bond is a very narrow one: it is a bond that conforms closely to the limit of extreme ionicity depicted in Fig. 2 C. Few, if any, materials meet this criterion for pure ionicity. Therefore, in our view, the breadth of his definition of covalency is problematic. It implies that the label 'ionic' is almost redundant as a descriptor of real materials and that applying the label 'covalent' to a material reveals almost nothing about how electrons are distributed within it or the nature of its interatomic forces. Therefore, we choose to define ionicity in energetic terms: *An ionic molecule or material is one whose energy differences and interatomic forces are well approximated by those of a set of slightly-overlapping polarizable ions.* The ions' charges need not be integers.

The electron clouds of the ions in an ionic bond must overlap. If they did not, there would be no repulsion to balance the cation-anion attraction. By 'slightly-overlapping' we simply mean that, as ions move, the change in the potential energy associated with the overlap only makes up a very small fraction of the total change in potential energy. This is the case if only a small fraction of the valence electron density resides where $\boldsymbol{\nabla} n$ is not directed towards the closest nucleas. When it is the case, even crude approximations to the overlap energy can be used to estimate energy differences and forces accurately. Pairwise models often suffice, but more accurate models have also been developed [57, 85].

Cohen's evidence for covalency is that Ti-O hybrid valence states exist and that the ions' charges are smaller than their formal values. Both of these are perfectly

consistent with our broader definition of ionicity. For example, the density corresponding to a hybrid valence state could comprise two disjoint pockets - one localized on Ti and the other on O. An electron in such a state would spend all of its time localized on ions, but it would share its time between Ti and O, contributing a fraction of its $-e$ charge to each species. Therefore, the ions' charges would be smaller than their formal values but an ionic model of energetics would still be appropriate. It is easier, more accurate, conceptually simpler, and better justified by theory [61, 86] to model the distortion of an ion by the local field from other ions by assigning a dipole moment to it in proportion to this field, than it is to model the same distortion within the framework of LCAO hybridization and covalency. Attempts to derive accurate models of bonding on the basis of the LCAO and tight binding theory have proved horrendously complex, and have failed to describe the bonding of crystalline silicon with accuracy comparable to ionic models of ionic materials [87]. There are, of course, many covalent effects that cannot be modelled accurately with an ionic model of energetics but, in at least some materials, apparent signatures of non-ionic covalent bonding have turned out to be the effects of ions being polarizable [88], or other small easily-modeled deviations from the rigid-ion limit [57, 69].

To support his claim that covalency helps to 'drive' the polar instability [89], Cohen showed that FE phases can be rendered unstable in calculations if hybridization of O 2p and Ti 3d states is inhibited by artificially increasing the energies of the Ti 3d orbitals [45, 51, 54]; a similar effect was demonstrated in $KNbO_3$ by penalising occupation of Nb 4d states [90]. Finally, he showed that BTO's FE phases are unstable if the energy of the crystal is calculated, not from the self-consistent ground state electron density, but from a superposition of electron densities of spherically-symmetric ions [45, 91].

The fact that ferroelectricity does not survive driving electrons from their ground state to a state in which ions' charges are larger by $50-100\%$ [45, 51, 54, 90], is also no less consistent with our definition of ionicity than it is with Cohen's definition of covalency. Ferroelectricity arises in BTO (and not in $SrTiO_3$, which is isoelectronic) from a delicate balance of energies and can easily be destroyed by slight compositional changes or strain. It is not surprising that this balance is disrupted by such enormous changes to the ions' charges because they would change the crystal's energetics in many ways. For example, they would increase the magnitude of the Madelung energy by $25-100\%$; they would change the electric susceptibility by increasing the O ions' polarizabilities; and they would increase the radius of the O ion by more than they reduce the radius of the Ti ion, which might leave less room to accommodate polar distortions. The results of Sec. III (Figs. 6 and 8) will help to illustrate just how large a perturbation a 50% increase in ions' charges is. They will show that carrier-induced changes in electronic structure, which are large enough to destabilize ferroelectricity, only change ions' charges by one or two percent.

It is also unsurprising, and perfectly consistent with our definition of ionicity, that preventing ions from polarising, as Cohen and Krakauer did when they calculated BTO's energy from a superposition of spherically-symmetric electron densities [45, 91], would make symmetry-lowering polar distortions energetically unfavourable. It is known that, by not allowing ions to polarize, the *potential induced breathing* model that they used drastically overestimates the energy cost of polar distortions, resulting in long-wavelength LO phonon frequencies that are much too high [92]. One reason for this is that polarization of the ions partially screens the long-wavelength electric field responsible for hardening the LO mode relative to the TO mode. Imposing spherical symmetry on ions' electron clouds would also change the short-range Ti-O interaction significantly because it prevents ions from deforming to lower the energy of electrons in the compressed bond. For all these reasons, we do not share Cohen's view that this finding, together with his other findings discussed above, constitute incontrovertible proof that BTO is covalent in a way that cannot be modelled accurately with an ionic model of energetics [89].

We have explained why Cohen's LCAO analysis of BTO's bonding is perfectly consistent with it being *energetically* ionic, but we are also in a position to make a stronger statement, based on previous work: Highly-accurate models of interatomic forces have been developed for the oxides BTO [49], MgO [57], SiO_2 [56], TiO_2 [59], Al_2O_3 [60], $MgSiO_3$ [93], GeO_2, Y_2O_3, and ZrO_2, by fitting the parameters of ionic models of bonding to their DFT-calculated PES's. If we measure ionicity by the closeness of the fit that can reproducibly be achieved by our ionic model to an effectively-infinite DFT dataset, the only one significantly more ionic than BTO is MgO. Extensive testing of ionic force fields for BTO show excellent agreement with DFT calculations and experiment on all calculated observables [49].

2. *Short-range vs long-range Coulomb forces*

It is common in the literature to find ferroelectricity attributed to *long-range* Coulomb interactions destabilizing a higher-symmetry non-polar parent phase [45, 53]. However, several recent works [94, 95] have suggested that BTO's phase diagram can be reproduced by models that neglect long-range Coulomb interactions: the only ingredients necessary are the Coulomb attraction between neighbouring ions, which drives polar distortions of individual unit cells, and an energy penalty for misalignment of polar distortions in nearby (within $\sim 1\,\mathrm{nm}$) unit cells [95]. Furthermore, the very existence of a polar metallic phase suggests that polar distortions are driven by the very strong attraction between anion and cation neighbours rather than by long-range fields, which would be screened by free carriers.

3. Simple model of energetics

We use the following simple picture to interpret experimental results and our calculations: Conduction band electrons (CBEs) are either bound to ions (Ti or O, but not Ba) or they are delocalized in interstices. CBEs bound to ions are bound more weakly, on average, than valence band electrons (VBEs) because their energies are higher. This increases ions' sizes and gives their outer electrons more freedom to screen local fields. The lower CB has mostly Ti 3d character, so bound CBEs reduce the Ti ion's charge. The upper VB has mostly O 2p character, so vacating it reduces the magnitude of the O ion's charge. Therefore, the CBEs bound to ions weaken the Ti-O attraction in two ways: they reduce the ions' charges and increase their polarizabilities. The CBEs delocalized in interstices, on the other hand, are those most responsive to applied or intrinsic long-range fields. Long range fields are relatively weak. For example, the force of attraction between point unit charges separated by 2 Å ($\approx$ Ti-O distance) is at least three orders of magnitude larger than the force that would be exerted on a unit charge by a field capable of causing dielectric breakdown in BTO ($\sim 10^7 - 10^8$ V m^{-1} [96, 97]).

We can approximate the potential energy difference per unit cell between any FE phase and the Pm$\bar{3}$m structure as $\Delta\mathcal{E} = \Delta\mathcal{E}^{\rm att} + \Delta\mathcal{E}^{\rm rep}$, where $\Delta\mathcal{E}^{\rm att} \leq 0$ is the energy of Ti-O attraction and $\Delta\mathcal{E}^{\rm rep} \geq 0$ includes inter-nuclear repulsion and exchange repulsion caused by overlap of the ions' electron clouds. In Pm$\bar{3}$m each Ti is equidistant from six O ions and $\Delta\mathcal{E}^{\rm rep}$ and $\Delta\mathcal{E}^{\rm att}$ take their minimum and maximum values, respectively, both of which are zero. At equilibrium $\Delta\mathcal{E} = \Delta\mathcal{E}_{\rm eq} = \Delta\mathcal{E}^{\rm rep}_{\rm eq} + \Delta\mathcal{E}^{\rm att}_{\rm eq} = \Delta\mathcal{E}^{\rm rep}_{\rm eq} - \left|\Delta\mathcal{E}^{\rm att}_{\rm eq}\right|$ and the partial derivatives of $\Delta\mathcal{E}^{\rm att}$ and $\Delta\mathcal{E}^{\rm rep}$ with respect to any nuclear or phonon coordinate are equal in magnitude and opposite in sign. This balance is disrupted when the Ti-O attraction is weakened, causing the equilibrium structure to move closer to the Pm$\bar{3}$m structure favoured by $\Delta\mathcal{E}^{\rm rep}$. This reduces the magnitudes of $\mathbf{P}$ and $\Delta\mathcal{E}_{\rm eq}$.

The magnitude of the latter, $|\Delta\mathcal{E}_{\rm eq}|$, is the potential energy barrier (per unit cell) that must be surmounted to switch the direction of $\mathbf{P}$ by rigid relative motion of the crystal's sublattices of inequivalent atoms. In reality, $\mathbf{P}$ does not switch direction in such an orderly manner. Nevertheless, we take the reduction of $|\Delta\mathcal{E}_{\rm eq}|$ to be indicative of equivalent changes to the high-dimensional PES on which the nuclei move. A weakening of the Ti-O attraction is expected to reduce the magnitudes of the PES's peaks and troughs in the vicinity of the equilibrium structures of the PE and FE crystals. Therefore, a lowering of $|\Delta\mathcal{E}_{\rm eq}|$ indicates a lowering of both E_c and T_C.

D. Populating the conduction band by doping and/or photoexcitation

Although calculations suggest that the band gaps of the Pm$\bar{3}$m and P4mm phases are indirect, with VB maxima at $\left(\frac{1}{2}, \frac{1}{2}, \frac{1}{2}\right)$ and CB minima at $\mathbf{\Gamma}$, their direct gaps at $\mathbf{\Gamma}$ are larger by only about 0.1 eV and 0.4 eV, respectively. Therefore, it can be viewed as a direct-gap semiconductor [112].

An ultrashort $\gtrsim E_g$ laser pulse would excite electrons from the upper VB to the lower CB, thereby creating two 'carrier' populations: CBEs and valence band holes (VBHs). Eventually, the electrons and holes will recombine, returning the electronic subsystem to thermal equilibrium, which is very close to its ground state.

As an alternative to creating a *transient* population of CBEs in pure BTO by photoexcitation, a fixed density of CBEs can be introduced during synthesis by $n-$doping. For example, by introducing some Nb^{5+} to Ti^{4+} sites, some La^{3+} or Y^{3+} to Ba^{2+} sites, or by introducing oxygen vacancies [17–19, 44, 98–100]. Cation n-dopants, having greater nuclear charges, are expected to retain more of their outer-shell electrons than the Ti and Ba cations that they replace. Oxygen vacancies are located at or near local maxima of the electric potential and so each vacancy is expected to trap some fraction of the nominal two CBEs that it introduces to the crystal, either in the vacancy or on nearby Ti cations [101, 102]. Therefore, although the nominal density of CBEs in the dilutely $n-$doped materials $La_yBa_{1-y}TiO_3$, $BaNb_yTi_{1-y}O_3$, and $BaTiO_{3-y/2}$ is y, the true density, $x(y)$, is lower due an unknown fraction of the electrons being trapped by their donors.

In doped BTO the x electrons per formula unit that are not bound to dopants are expected to affect the electronic structure in similar ways to photoexcited CBEs. They are expected either to bind loosely to Ti cations or O anions, thereby weakening the Ti-O attraction, or to be delocalized and responsive to weak long-range fields.

There are several obvious differences between $n-$doped BTO and photoexcited BTO. One difference is that dopants and vacancies perturb the crystal structure locally. Another difference is that in photoexcited BTO there are two species of charge carrier, CBEs and VBHs, that can respond to long-range fields. Even if holes were immobile it might be important that the positive charges that compensate for photoexcited CBEs are holes, which are located predominantly on oxygen anions, whereas the CBEs in doped BTO are compensated by positively-charged oxygen vacancies or by the greater charges of dopant nuclei.

Although these differences may have some important consequences, the primary qualitative effects of the CBEs are expected to be the same in all cases: the short range Ti-O attraction is weakened by those that bind to Ti and O ions, and conductivity/screening is enhanced by those that are delocalized in interstices. Therefore, although our calculations were designed to study photoex-

cited BTO, they shed substantial light on doped BTO and allow us to explain many of its observed properties.

We are motivated to try because recent experiments on n-doped BTO show that metallicity and ferroelectricity can coexist [17–19]. It has been found that in n-doped BTO the phase transition temperatures are decreased [17, 44, 98] and the magnitudes of off-centre ferroelectric distortions are significantly reduced [17–19]. Also, a remarkable softening of the SM is observed, along with an overdamped low-frequency CM component [44]. We find that our calculations and our simple ionic picture of bonding and energetics allow us to offer plausible explanations for all of these observations.

E. Displacive excitation of coherent phonons (DECP)

During and immediately after absorption of a laser pulse the populations of CBEs and VBHs are in non-thermal states; however, they typically decohere and thermalize very quickly ($\lesssim$ 100 fs) [103, 104]. What happens next depends strongly on the crystal's symmetry and on the time scales for the multifarious relaxation processes which, eventually, return the subsystems of electrons and phonons to a mutual thermodynamic equilibrium. Electron-hole recombination typically takes nanoseconds [103, 105]. Therefore, if diffusion of CBEs and VBHs away from the irradiated region is slow enough, their number densities remain approximately constant on phonon time scales (picoseconds). Rapid decoherence and thermalization of fixed densities of CBEs and VBHs imply that the material establishes a new *quasi*-equilibrium electronic state within 100s of femtoseconds (fs). This means that the character of the bonding in the material, and therefore its phonon frequencies and equilibrium bond lengths, are changed. If the material is crystalline and possesses A_1 phonon modes, the equilibrium A_1 mode coordinates change in much less than a phonon period. Zone-center coherent A_1 phonon oscillations, with a cosine-like time dependence, ensue as they move towards their new equilibria and oscillate about them. This phenomenon, which is schematized for BTO in Fig. 3, is known as *displacive excitation of coherent phonons* (DECP) [106]; it can be observed experimentally as modulations of the optical response to time-delayed probe pulses. Much can be learned about the phonons' interactions with other degrees of freedom from the damped oscillations of the differential reflectivity or transmissivity [107].

As discussed above, in its ferroelectric phases BTO possesses three optically-active A_1 phonon modes and the CM, which is characterised by strongly-damped large-amplitude fluctuations along the A_1 FM eigenvector between quasi-stable off-centre ionic positions [108]. In principle, DECP excites all A_1 modes to some degree. As the FM/SM is characterised by the countermotion of Ti and its O_6 cage, it is obvious that, by weakening the Ti-O attraction, photoexcitation would excite it. Physical mechanisms for direct excitation of the LM or the AM are not readily apparent.

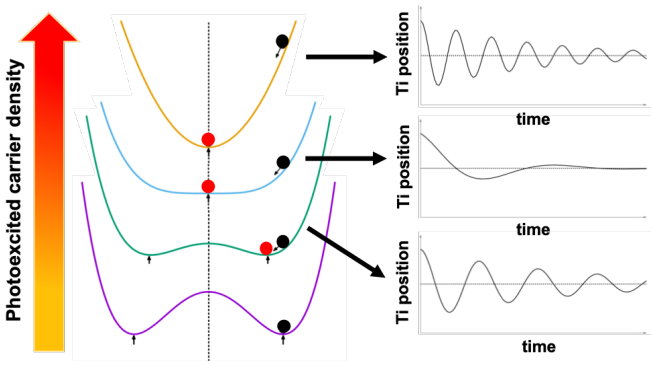

FIG. 3. Schematic. Left: Potential energy as a function of Ti position in the ground state and at three levels of photoexcitation, with their equilibrium positions indicated by black and red dots, respectively. Right: Oscillations due to the near-instantaneous shift of the equilibrium Ti position.

At high levels of photoexcitation, the amplitude of the coherent FM phonon would be large enough for the barrier between the symmetry-equivalent $\mathbf{P}$ and $-\mathbf{P}$ states to be surmounted; in that case the CM would be excited instead of, or as well as, the FM, and very rapid decoherence and decay of the displacively-excited lattice motion is expected.

II. THEORY AND METHODS

To study the transient ($\ll$ ns) effects of an ultrashort $>E_g$ pulse on structure and dynamics, we performed constrained density functional theory (DFT) calculations. We used an approach that has been used successfully to model a number of other materials [109–111]. It is based on several physical assumptions and simplifications, which we explain below.

We do not attempt to describe all details of the photoexcitation and relaxation processes. Some of these, such as the energy of the exciting photons, become irrelevant when carrier thermalization erases memory of them. Others are easily accounted for; for example, if some mobile charge carriers form excitons [112], the number contributing to conductivity measurements is reduced. Many others might have quantitative effects that are less easy to calculate, but they are unlikely to alter the simple premise on which our conclusions are built, namely, that CBEs weaken the Ti-O attraction and increase conductivity. Therefore, consideration of their effects is unlikely to alter the physical picture qualitatively.

A. Assumptions used to model the photoexcited state

We assume that electrons reach a *quasi*-equilibrium number density $n(\mathbf{r}\,;x)$, where x is the average photoexcited CBE and VBH density, within 100's of fs of pulse absorption. Our calculations use the simplification that this *quasi*-equilibrium state is reached instantaneously. We assume that x remains constant for several ps after pulse absorption and that it is approximately uniform throughout a mesoscopic ($\gg$ nm) region of the crystal. We assume that the excited state responds adiabatically to nuclear motion. On the picosecond time scale of interest to us, we assume that most of the energy absorbed from the laser pulse remains in the electronic subsystem, which means that the rates at which it is lost by radiative carrier-recombination, phonon emission and diffusion of carriers are low [105, 113].

B. Occupation numbers

We treat electrons and holes as independent particles occupying states $\{\phi_i\}$ with probabilities $\{f_i\}$ and $\{1-f_i\}$, respectively; the electron density is $n(\mathbf{r};x) \equiv \sum_i f_i(x)|\phi_i(\mathbf{r};x)|^2$. To determine the occupation numbers, $\{f_i\}$, we maximise the entropy of single-electron state occupation, $S[\{f_i\}]$, subject to the following constraints: the total energy of the electronic subsystem is conserved and both the total number of electrons per unit cell (N) and the number of electrons in the conduction band per unit cell (x) are conserved. Therefore the functional

$$\mathfrak{F} \equiv \lambda_S S[\{f_i\}] + \lambda_E E[n] + \lambda_N^{(h)} \sum_{i\leq N}(1-f_i) + \lambda_N^{(e)} \sum_{i>N} f_i \tag{1}$$

is made stationary with respect to $\{\phi_i\}$ and $\{f_i\}$, where λ_E/λ_S, $\lambda_N^{(v)}/\lambda_S$ and $\lambda_N^{(c)}/\lambda_S$ are Lagrange multipliers and $E[n]$ is the energy of the electrons in the presence of the Coulomb potential from the nuclei. We include four λ_* constants in Eq. 1 instead of three to make clear that stationarity of $\mathfrak{F}$ can either mean that S is stationary at a fixed value of E or that E is stationary at a fixed value of S. In the latter case the Lagrange multipliers have the form λ_*/λ_E instead of λ_*/λ_S, but the mathematical form of the f_i's derived from Eq. 1 is not changed. The constants appearing in this form (Eqs. 2) are determined by the values of the constrained quantities.

Our derivation requires an expression for S. Therefore, let us assume that the photoexcited region consists of P primitive unit cells, so that each of the single-electron states is P-fold degenerate, and that each of these P states is either occupied by one electron or empty. If p_i is the number of states that are occupied in the i^{th} set of P-fold degenerate states, the Boltzmann entropy associated with the occupations of this set of states is $S_i = k_B \log W_i$, where W_i is the number of different ways to occupy p_i of the P states.

$$S_i = k_B \log \left({}^P C_{p_i}\right) = k_B \log\left(\frac{P!}{p_i!(P-p_i)!}\right)$$

Since P is very large, we can use Stirling's approximation, $\log P! \approx P\log P - P$, and this becomes

$$S_i = k_B\left[P\log(P) - (P-p_i)\log(P-p_i) - p_i\log(p_i)\right]$$

The occupation entropy associated with the i^{th} band can then be found by dividing S_i by P; and the total occupation entropy per unit cell is found by summing over all bands, dividing by P, and noting that $f_i = p_i/P$. The result is

$$S = \frac{1}{P}\sum_i S_i = \sum_i -k_B\left[\, f_i\log(f_i) + (1-f_i)\log(1-f_i)\right]$$

With this expression for the occupation entropy, stationarity of $\mathfrak{F}$ with respect to f_i implies that

$$f_i = \begin{cases} \left[e^{(\epsilon_i-\mu_e)/k_B\tau}+1\right]^{-1}, & \text{for } i > N \\ \left[e^{(\epsilon_i+\mu_h)/k_B\tau}+1\right]^{-1}, & \text{for } i \leq N \end{cases} \tag{2}$$

where $\tau \equiv -\lambda_S/\lambda_E$, $\mu_e \equiv \tau\,\lambda_N^{(e)}/\lambda_S$, $\mu_h \equiv \tau\,\lambda_N^{(h)}/\lambda_S$, and

$$\epsilon_i \equiv \left.\frac{\partial E}{\partial f_i}\right|_{\{\phi_j\},\{f_j\}_{j\neq i}} \implies \left.\frac{\partial E}{\partial(1-f_i)}\right|_{\{\phi_j\},\{f_j\}_{j\neq i}} = -\epsilon_i$$

For non-interacting electrons [holes], ϵ_i [$-\epsilon_i$] can be interpreted as the energy of the i^{th} single electron [hole] state. From Eq. 2 we see that the CBEs and VBHs have separate Fermi-Dirac distributions with different chemical potentials (μ_e and μ_h, respectively) and a common temperature τ. Given τ and the set of single particle energies $\{\epsilon_i\}$, the values of μ_e and μ_h can be determined from the constraints $\sum_{i>N} f_i = \sum_{i\leq N}(1-f_i) = x$ using a bisection method.

The temperatures of electrons and holes are the same because, for simplicity, we have constrained the total electronic energy E, rather than separately constraining the energies of electrons and holes. We justify this simplification empirically by verifying that the results of our calculations are insensitive to τ as long as it is large enough to smooth out the discontinuities in the dependence of E on nuclear positions caused by discrete sampling of the Brillouin zone (see Fig. 5). More generally, apart from this jitter when τ is low or the sampling grid is coarse, we have found that, for a given value of x, our results are largely insensitive to the details of excited state occupation. We attribute this to the fact that the qualitative effects of occupying [vacating] the lower CB [upper VB] are always to reduce the Ti-O attraction and to create delocalized charge carriers.

To calculate forces, equilibrium structures, and phonon frequencies in the photoexcited state we must specify how τ depends on the set $\underline{\mathbf{r}}$ of nuclear positions. One approach

is to assume that τ is independent of $\underline{\mathbf{r}}$. Physically, this implies that the carriers are in contact with a heat bath - an assumption that might be appropriate in the limit of high carrier thermal conductivity if the spot size of the probe pulse is much smaller than that of the pump pulse, or if the single electron energies are insensitive to $\underline{\mathbf{r}}$. We use a different approach, which is to assume that S is independent of $\underline{\mathbf{r}}$. This implies that nuclei change E by doing work on the carrier subsystems as they move. Physically, both the constant-τ and the constant-S approaches are simplistic limiting cases; however, we have checked that our results do not depend strongly on which approach is used.

Note that when τ has been determined and $\mathfrak{F}$, and hence $\mathfrak{F}/\lambda_E$, are stationary, the electronic free energy $\mathcal{F} \equiv E - \tau S$ is also stationary, subject to the constraints on the numbers of carriers.

C. Computational methods and calculation parameters

We used the **ABINIT** package [114, 115] with the projector-augmented wave (PAW) method [116], and the (ground state) PBEsol exchange-correlation functional [117]. We step outside the domain in which DFT has formally been justified by treating the Kohn-Sham eigenstates ($|\phi_i\rangle$) and eigenvalues (ϵ_i) as independent-electron states and energies, respectively. We expanded the wavefunctions and core charge density using plane waves up to energy cutoffs of 980 eV and 1360 eV, respectively.

To achieve stationarity of $\mathfrak{F}$ with respect to variations of $\{\phi_i\}$ and $\{f_i\}$, we iterate them to self-consistency: at each iteration we find the set of eigenfunctions and eigenvalues of the Kohn-Sham hamiltonian $\hat{h}[n]$ calculated from the electron density (n) at the previous iteration. We determine $\{f_i\}$ from the eigenvalues as follows: we use a bisection method to determine the value of τ that gives the desired entropy S_x at the desired carrier density x; at each step of the bisection algorithm used to determine τ, two nested bisection algorithms are used to determine the values of μ_e and μ_h for which the numbers of CBEs and VBHs per $BaTiO_3$ formula unit are both x. Once mutually-consistent values of τ, μ_e, and μ_h have been determined, the ϕ_i's and the Fermi-Dirac f_i's are used to update $n(\mathbf{r}\,;x)$ [109–111]. When $n(\mathbf{r}\,;x)$ has been iterated to self-consistency, $\mathcal{F}$ is stationary with respect to variations of occupation numbers and eigenfunctions that preserve x and S_x.

The PES on which the nuclei in the unit cell are assumed to move is $\mathcal{E}_x(\underline{\mathbf{r}}) \equiv E_{nn}(\underline{\mathbf{r}}) + \mathcal{F}(\underline{\mathbf{r}}, x)$, where E_{nn} is the Coulomb energy of repulsion between nuclei. The stationarity of $\mathcal{F}$ implies that a Hellmann-Feynman theorem can be used to calculate forces on nuclei. Fig. 4 verifies that, for $x = 4.0\ e^-/\text{f.u.}$, the Hellmann-Feynman forces coincide with the forces calculated numerically from finite differences of $\mathcal{E}_x$, and that they differ slightly from forces calculated from finite differences of $\mathcal{E}_x + \tau S = E_{nn} + E$. This demonstrates that constraining S_x and x at each step of the iteration to self-consistency ensures stationarity of $\mathfrak{F}$.

Y	$s^1_{\rm Y}$	$s^2_{\rm Y}$	$s^3_{\rm Y}$
Ba	0	0	0
Ti	$\frac{1}{2}+\delta_{\rm Ti}$	$\frac{1}{2}+\delta_{\rm Ti}$	$\frac{1}{2}+\delta_{\rm Ti}$
O_1	$\frac{1}{2}+\delta_{\rm O_I}$	$\frac{1}{2}+\delta_{\rm O_I}$	$\delta_{\rm O_{II}}$
O_2	$\frac{1}{2}+\delta_{\rm O_I}$	$\delta_{\rm O_{II}}$	$\frac{1}{2}+\delta_{\rm O_I}$
O_3	$\delta_{\rm O_{II}}$	$\frac{1}{2}+\delta_{\rm O_I}$	$\frac{1}{2}+\delta_{\rm O_I}$

TABLE I. Equilibrium lattice coordinates $\mathbf{s}_{\rm Y} = (s^1_{\rm Y}, s^2_{\rm Y}, s^3_{\rm Y})$ of the atoms (Y $\in \{\text{Ba}, \text{Ti}, \text{O}_1, \text{O}_2, \text{O}_3\}$) in perfect R3m and Pm$\bar{3}$m crystals. In Pm$\bar{3}$m all three δ_* parameters are zero. In the R3m phase we calculate ground state ($x = 0$) equilibrium values of $\delta^{\rm eq}_{\rm Ti,0} = 0.0112$, $\delta^{\rm eq}_{\rm O_I,0} = -0.0113$, and $\delta^{\rm eq}_{\rm O_{II},0} = -0.0181$.

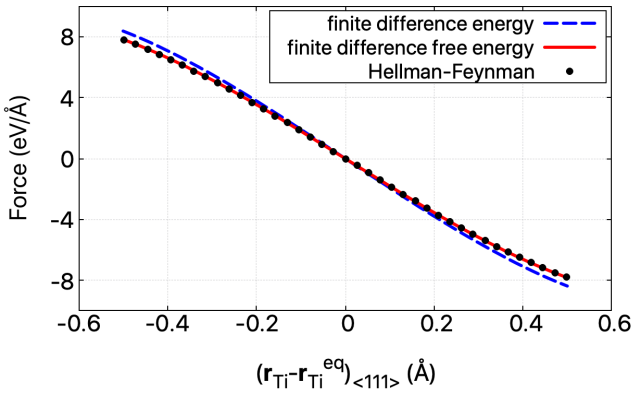

FIG. 4. Hellmann-Feynman force on a Ti atom in our model of photoexcited BTO ($x = 4\ e^-/\text{f.u.}$) as a function of its displacement from equilibrium along $\langle 111\rangle$ (red dots) compared to forces calculated from finite differences of $E_{nn} + E$ (dashed black line) and $E_{nn} + \mathcal{F}$ (blue line).

At each value of x we chose S_x to be equal to the value of S at $\tau = 0.02\ \text{eV}/\text{k}_\text{B}$ when the lattice coordinates of the atoms, but not necessarily the lattice vectors, are those of the ideal Pm$\bar{3}$m crystal quoted in Table I. This is our reference structure and we denote the change in $\mathcal{E}_x$ with respect to its value in this structure by $\Delta\mathcal{E}_x$.

Because the surrounding crystal inhibits overall strain of the photoexcited region, and because our primary interest is in optical phonons and polar structural distortions in the long-wavelength limit, in all calculations except those presented in the inset of Fig. 6, we fixed the lattice vectors of the primitive unit cell to their ground state ($x = 0$) equilibrium values in the low-T R3m phase.

To study the effects of photoexcitation on phonon frequencies and structural stability, phonons were calculated at different values of x. We used *Phonopy* [118]

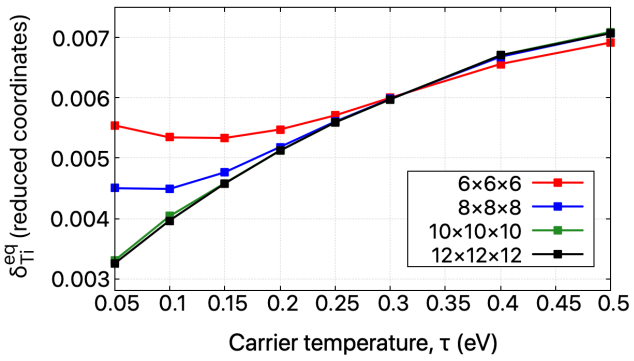

FIG. 5. The parameter, $\delta^{\rm eq}_{\rm Ti}$, that defines the equilibrium Ti lattice coordinates in the R3m phase as a function of carrier temperature (τ) when the Brillouin zone is sampled with a uniform $n_k \times n_k \times n_k$ grid, where $n_k \in \{6, 8, 10, 12\}$.

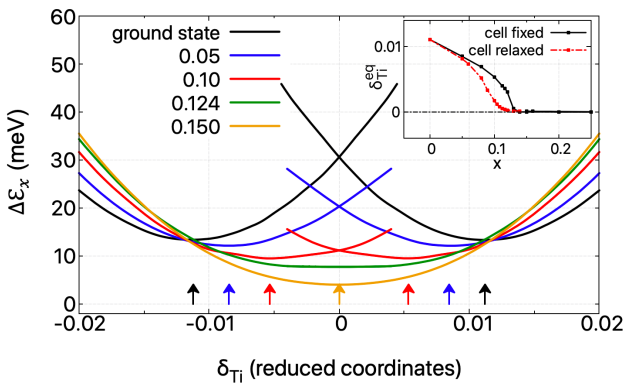

FIG. 6. Potential energy, $\Delta\mathcal{E}_x$, as a function of $\delta_{\rm Ti}$, where $(\delta_{\rm Ti}, \delta_{\rm Ti}, \delta_{\rm Ti})$ is the displacement of the Ti sublattice, in lattice coordinates, from its position in a perfect Pm$\bar{3}$m crystal. Results are presented for the electronic ground state and at three levels of photoexcitation (x). Arrows indicate the locations, $\pm\delta^{\rm eq}_{{\rm Ti},x}$, of the curves' minima and the curves are shifted vertically to intersect at the ground state minimum, $\delta^{\rm eq}_{{\rm Ti},0}$. Inset: Comparison of $\delta^{\rm eq}_{{\rm Ti},x}$ versus x for a fixed ground state cell (black curve) and for a fully-relaxed cell (red curve).

to calculate and diagonalize the dynamical matrix constructed from finite-differences of forces in a $3 \times 3 \times 3$ supercell. For technical reasons, and physical reasons related to mobile carriers in photoexcited states, we did not apply long-range field corrections to the dynamical matrix in any of our calculations, including our ground state calculations. Therefore, the giant LO-TO splitting expected for the SM [119] is absent.

We sampled the Brillouin zone using uniform $8 \times 8 \times 8$ and $2 \times 2 \times 2$ grids for calculations on primitive unit cells and $3 \times 3 \times 3$ supercells, respectively. The grids were shifted away from $\mathbf{\Gamma}$ by half a grid-spacing along each reciprocal lattice vector. We checked that our results were converged with respect to the density of $k-$points and were insensitive to τ at these values. The results of one such test are presented in Fig. 5.

III. RESULTS

A. Ground state structure

We first found the equilibrium structure in the ground state ($x = 0$) by simultaneously relaxing the lattice vectors and atomic positions. The resulting structure is in excellent agreement with experiments [24] and previous DFT calculations [24, 120, 121]: it has R3m symmetry, the lattice parameter is $a = 4.00$ Å, and the rhombohedral angle is 89.86°; the lattice coordinates of the atoms are provided in Table I in terms of parameters $\delta_{\rm Ti}$, $\delta_{\rm O_I}$, and $\delta_{\rm O_{II}}$, which specify the differences between the lattice coordinates of the Ti and O atoms in the R3m FE phase and its higher-symmetry parent PE phase, Pm$\bar{3}$m.

B. Excited state structure and energetics

With lattice vectors fixed at their ground state equilibrium values, and for a range of values of x, we calculated the variation of $\Delta\mathcal{E}_x$ with respect to the $\langle 111\rangle$ displacement parameter, $\delta_{\rm Ti}$, of the Ti sublattice. At each value of $\delta_{\rm Ti} \in [-0.02, 0.02]$ we kept Ba and Ti atoms fixed at the lattice coordinates of Table I and relaxed the O atoms before calculating $\Delta\mathcal{E}_x\,(\delta_{\rm Ti})$. The results are plotted in Fig. 6 for five values of x, including $x = 0$. There are two minima, which correspond to Ti displacements parallel and antiparallel to $\mathbf{P}$; they are located at $\delta_{\rm Ti} = \pm\delta^{\rm eq}_{{\rm Ti},x}$, where superscript 'eq' abbreviates *equilibrium* and subscript 'x' is the carrier density. As x increases the two symmetry-equivalent wells get shallower and their minima move closer together until, above a critical carrier density $x_c \approx 0.124\ e^-/\text{f.u.} \approx 1.9 \times 10^{21}\ e^-/\,\text{cm}^3$, the wells have merged into a single potential energy basin located at $\delta_{\rm Ti} = \delta^{\rm eq}_{{\rm Ti},x>x_c} = 0$. Therefore, above x_c the FE distortion is no longer energetically favourable and the structure that minimises $\mathcal{E}_x$ is Pm$\bar{3}$m, for which $\mathbf{P} = 0$.

Our calculated value of x_c is close to the values ($\sim 0.10 - 0.11\ e^-/\text{f.u.}$) calculated by others [94, 122], despite significant differences in how single-electron states are occupied in our calculations: VB states were fully occupied in previous calculations and, instead of the CBEs' negative charges being compensated by VBHs, it was compensated by a positive uniform background charge density [55, 94, 122] or, in supercell calculations, by dopant nuclei [122]. Our value of x_c also appears consistent with experimental estimates and measurements of the critical carrier density at which ferroelectricity disappears [17, 44]. However in our calculations x_c is the

critical density of CBEs, whereas the critical densities reported by experimentalists tend either to be densities of mobile electrons measured using the Hall effect, or the nominal density of extra electrons provided by dopants, i.e., integer × dopant density. In the dilute doping limit ($x \to 0$) the nominal density should be viewed as an upper bound on the density of CBEs because vacancies and dopants bind some of the extra valence electrons that they introduce to their host BTO crystal. The carrier density from a Hall measurement, on the other hand, seems likely to be a lower bound on the density of CBEs if, as our calculations suggest, a high proportion of the CBEs remain bound to Ti or O ions.

It is clear from Fig. 6 that $\left|\delta^{\rm eq}_{{\rm Ti},x}\right|$ and the potential energy gained from the ferroelectric distortion, $D_x \equiv |\Delta\mathcal{E}_x(\delta^{\rm eq}_{{\rm Ti},x})|$, both decrease with increasing carrier density, x. The distances of the oxygen atoms from their high-symmetry positions also decrease. The values of $(D_x, \delta^{\rm eq}_{{\rm Ti},x})$ when x is $0.00\,e^-/\,$f.u., $0.05\,e^-/\,$f.u., and $0.10\,e^-/\,$f.u. are, respectively, (16.64 meV, 0.0112), (8.18 meV, 0.0084), and (1.67 meV, 0.0053). Assuming that CBEs do not increase ions' Born effective charges significantly, the reduction in the magnitude of the polar distortion implies a reduction in the magnitude of $\mathbf{P}$.

D_x quantifies the stability of the FE phase over the PE phase in the $T \to 0$ limit and its reduction with x implies that photoexcitation makes R3m less stable and lowers the energy barrier to reversing $\mathbf{P}$ by rigidly displacing the Ti and O sublattices relative to the Ba sublattice. Therefore photoexcitation weakens ferroelectricity and, above $x \approx x_c$, the ferroelectric state is not even stable in the $T \to 0$ limit. We found results qualitatively similar to those presented in Fig. 6 when we repeated our calculations with Ti displaced along $\langle 001\rangle$ and $\langle 011\rangle$.

As discussed in Sec. I A, the FE distortion is a superposition of displacements along A_1 eigenvectors. Therefore the dependence of $\delta^{\rm eq}_{{\rm Ti},x}$ on x implies a dependence of the equilibrium A_1 mode coordinates on x. Our assumption that electrons settle into their *quasi*-equilibrium photoexcited state within 100's of fs of absorbing a $> E_g$ laser pulse implies that the bonding changes within a small fraction of a phonon period. Effectively, the laser pulse suddenly renders A_1 modes out of equilibrium, which causes them to move towards their new equilibria and oscillate about them with the cosine-like time dependence (max. displacement at $t = 0$) that is characteristic of the DECP mechanism. For $x < x_c$ the energy wells in Fig. 6 become shallower and less symmetric as x increases. This suggests that in the long-wavelength limit the displacively-excited A_1 FM phonons have lower frequencies and are more anharmonic than their $x = 0$ counterparts. Therefore, a significant reduction of x during the lifetime of a coherent A_1 oscillation might be observable as an increasing frequency. When $x \approx x_c$ (green curve) the double-well has disappeared and $\Delta\mathcal{E}_x(\delta_{\rm Ti})$ has a single flat-bottomed (quartic) basin centered at $\delta_{\rm Ti} = 0$, which means that the crystal has become paraelectric ($Pm\bar{3}m$) in the $T \to 0$ limit. As $x > x_c$ increases further, the quartic potential becomes supplemented, and gradually dominated, by a quadratic confining potential of increasing curvature (orange curve).

Referring to the simple model discussed in Sec. I C 3, our results are consistent with photoexcitation reducing $\left|\Delta\mathcal{E}^{\rm att}_{\rm eq}/\Delta\mathcal{E}^{\rm rep}_{\rm eq}\right|$, thereby increasing the energy of the FE phase, which $\Delta\mathcal{E}^{\rm att}$ favours, relative to the $Pm\bar{3}m$ phase favoured by $\Delta\mathcal{E}^{\rm rep}$. We cannot calculate $\Delta\mathcal{E}^{\rm rep}$ to determine how sensitive it is to x, but we know that it includes an $x-$independent contribution from the Coulomb repulsion between nuclei and an $x-$dependent contribution from the kinetic energy and mutual repulsion of electrons in the compressed bond. We also know from the symmetry of $Pm\bar{3}m$ that $\Delta\mathcal{E}^{\rm att}(\delta_{\rm Ti}) = \Delta\mathcal{E}^{\rm att}(-\delta_{\rm Ti})$ and $\Delta\mathcal{E}^{\rm rep}(\delta_{\rm Ti}) = \Delta\mathcal{E}^{\rm rep}(-\delta_{\rm Ti})$, which means that $\Delta\mathcal{E}$ is stationary at $\delta_{\rm Ti} = 0$ and has the Taylor expansion

$$\Delta\mathcal{E}(\delta_{\rm Ti}) = \frac{1}{2}\delta^2_{\rm Ti}\left[\left(\Delta\mathcal{E}^{\rm att}\right)''(0) + \left(\Delta\mathcal{E}^{\rm rep}\right)''(0)\right] + \mathcal{O}\left(\delta^4_{\rm Ti}\right) \tag{3}$$

where two primes indicate a second derivative with respect to $\delta_{\rm Ti}$. By approximating $\Delta\mathcal{E}^{\rm rep}$ as a sum of pairwise repulsive interactions between Ti and its six equidistant O neighbours, it is easy to show that $\left(\Delta\mathcal{E}^{\rm rep}\right)''(0) > 0$. It then follows from the stability of R3m at low T that $\left(\Delta\mathcal{E}^{\rm att}\right)''(0) < 0$ and $\left|\left(\Delta\mathcal{E}^{\rm att}\right)''(0)\right| > \left(\Delta\mathcal{E}^{\rm rep}\right)''(0)$ when $x < x_c$.

$Pm\bar{3}m$ is lower in energy than R3m when $x > x_c$, which implies that, to leading order in $\delta_{\rm Ti}$, $\Delta\mathcal{E}$ is quartic when $x = x_c$ and quadratic when $x > x_c$. This is consistent with the curves plotted in Fig. 6 which appear quadratic when $x < x_c$ or $x > x_c$ and quartic when $x \approx x_c$. When $x > x_c$, $\left(\Delta\mathcal{E}^{\rm rep}\right)''(0) > \left|\left(\Delta\mathcal{E}^{\rm att}\right)''(0)\right|$, and $\Delta\mathcal{E}(\delta_{\rm Ti})$ has a positive quadratic term whose coefficient increases as the Ti-O attraction weakens with increasing x. The increase in curvature of $\Delta\mathcal{E}(\delta_{\rm Ti})$ suggests that, in the long-wavelength limit, the SM frequency increases with x. The softening of the FM band the hardening of $Pm\bar{3}m$'s SM below and above $x = x_c$, respectively, are confirmed in Fig. 9.

C. Photoinduced changes in electron density

Based on what we know about the characters of the upper VB and lower CB, and the assumption that bonding is ionic, we have suggested two simple ways in which populating the CB with electrons can destabilize ferroelectricity by weakening the Ti-O attraction. The first is that promoting electrons to the CB moves electrons from O to Ti, thereby reducing $|q_{\rm O}|$ and $q_{\rm Ti}$. The second is that CBEs are bound more loosely to ions than VBEs, which gives them more freedom to partially screen the Ti-O attraction. Simply put, at any finite separation the magnitude of the net Coulomb force between polarizable ions is less than that between rigid ions. However, this is no longer true in the large separation limit because fields

from multipoles have a relatively short range. Therefore, this way of destabilizing ferroelectricity would not apply if the FE instability is caused by long-range Coulomb interactions.

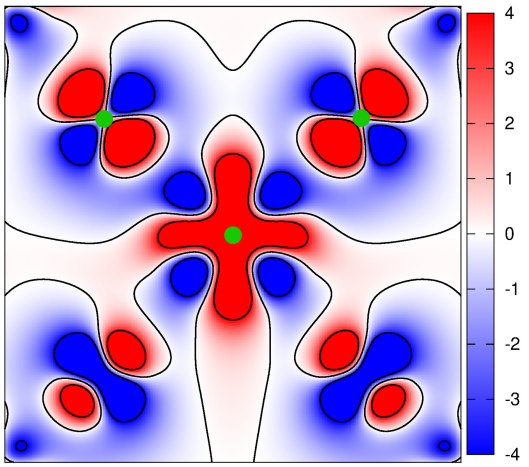

FIG. 7. Difference, $\Delta n(\mathbf{r}, 0.01)$, between the electron densities at $x = 0.01\ e^-/\text{f.u.}$ and $x = 0$ on the common plane of a Ti nucleus and its closest O neighbours (green spots). The color scale units are $10^{-4}\ e^-/\text{f.u.}$ and contour lines are drawn at $\Delta n = \pm 0.0004\ e^-/\text{f.u.}$ and at $\Delta n = 0$.

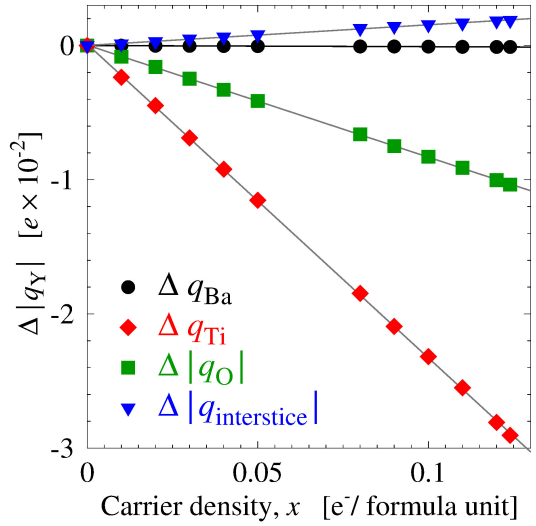

FIG. 8. Changes in magnitudes of ionic and interstitial charges as a function of carrier density.

We now justify our assumptions about bonding, and how photoexcitation affects it, by examining how the electron density $n(\mathbf{r}; x)$ changes with x. The difference, $\Delta n(\mathbf{r}\,; x) \equiv n(\mathbf{r}\,; x) - n(\mathbf{r}\,; 0)$, between the $x = 0.01\ e^-/\text{f.u.}$ excited state and the ground state is plotted in Fig. 7. It shows that photoexcitation takes electrons out of the O $2p$-like states whose axes are perpendicular to the Ti-O bond and that some of this density moves to Ti, some of it moves to O, and some is delocalized in interstices. To quantify, roughly, the changes in the ions' charges with x, we integrated the charge within atom-centered partitions, defined as follows: the point $\mathbf{r}_\text{Y} + \mathbf{R}$ is assigned to atom Y, where $\mathbf{r}_\text{Y}$ is the position of its nucleus, if *both* $\boldsymbol{\nabla} n\big|_{\mathbf{r}_\text{Y}+\mathbf{R}} \cdot \mathbf{R} < 0$ *and* $|\mathbf{R}| < R_\text{Y}$, where $R_\text{Ba} = 1.5\,\text{Å}$ and $R_\text{Ti} = R_\text{O} = 1.4\,\text{Å}$. Points not assigned to atom-centered partitions are assigned to interstices. Figure 8 shows that q_Ba does not change with x, that q_Ti and $|q_\text{O}|$ both decrease with x, and that $|q_\text{interstice}|$ increases with x. Although the charges ($q_\text{Ba} \approx 1.1\,e$, $q_\text{Ti} \approx 2.2\,e$, $q_\text{O} \approx q_\text{interstice} \approx -1.1\,e$) depend on the cut-off radii, the slopes of $\Delta|q_\text{Y}|(x)$ all vary by less than 15% in the range $R_\text{Y} \in [1.3\,\text{Å}, 1.6\,\text{Å}]$. The number of electrons excited into interstices per unit volume is approximately $1.50 \pm 0.05\,\%$ of x.

Despite our use of a crude and somewhat arbitrary method of estimating changes in ionic charges, Fig. 8 validates our assumption that photoexcitation reduces q_Ti and $|q_\text{O}|$, and shows that it also creates a low density of more delocalized, and therefore more mobile, interstitial or 'unbound' electrons.

It is very difficult to calculate, or even to define, excited-state atomic polarizabilities. However, we do not need to calculate them to know that if two identical nuclei have the same number of electrons bound to them, the one whose electrons are higher in energy is more polarizable. Higher energy electrons are more delocalized and, on average, are attracted more weakly to the ion's core. Photoexcitation changes the numbers of electrons bound to Ti and O slightly, while increasing their average energies. The polarizability of Ti is increased by both the number of electrons bound to it increasing and the average energy of those electrons increasing. We cannot be certain that the polarizability of O increases because it loses some of its electrons. Regardless of whether or not one chooses to discuss photoexcitation under the assumption of ionicity, it is clear from Figs. 7 and 8 that, apart from the creation of a small number of interstitial electrons, the major effect of photoexcitation is to redistribute, and increase the energies of, the electrons in the Ti-O bond. This weakens the bond.

When the number of delocalized, and therefore more mobile, interstitial electrons is sufficiently large, metallic conductivity is to be expected. When that happens the mobile electrons would screen long-range fields and so any long-range contribution to $\Delta\mathcal{E}^\text{att}$ should vanish. Therefore, the fact that a polar metallic phase has been observed experimentally appears to support the idea that $\Delta\mathcal{E}^\text{att}$ is dominated by the attraction between Ti and O neighbours. Interstitial electrons, as we have defined them, do not penetrate the Ti-O bond and would have a minimal effect on this attraction. Therefore polar distortions of individual unit cells could still lower the potential energy of the crystal and stabilize the FE phase. However, screening by free electrons would weaken the long-range elastic and electrostatic forces responsible for aligning the cell's polar displacements into a $\mathbf{P}-$field. By

lessening the degree of alignment, mobile electrons are expected to reduce the magnitude of $\mathbf{P}$. This would be the case even if $\Delta\mathcal{E}^{\rm att}$ was not weakened by photoexcitation.

These considerations suggest that a polar metallic phase can only exist if photoexcitation or doping generate enough interstitial electrons for metallic conductivity before the Ti-O attraction is weakened to the point that $\left|(\Delta\mathcal{E}^{\rm att})''(0)\right| < (\Delta\mathcal{E}^{\rm rep})''(0)$. They also suggest that metallic conductivity would reduce the $\mathbf{d}-\mathbf{d}$ correlation length, leading to increased disorder (reduced polarization anisotropy) in a polar metallic phase.

D. Selective excitation of the FM and CM

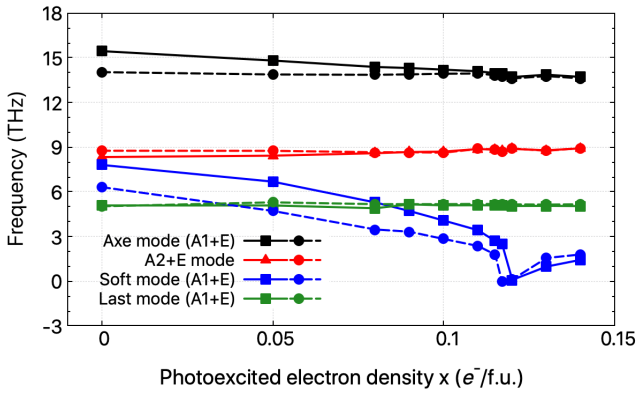

FIG. 9. Frequencies of $\mathbf{\Gamma}$-point optical phonons (without long-range field corrections to LO modes) as a function of photoexcited electron density, x (e^-/ f.u.).

Fig. 9 demonstrates that the SM frequency, $\nu_{\rm SM}$, depends strongly and non-monotonically on x. Specifically, it shows that $\nu_{\rm SM}\to 0$ as $x\to x_c$ and $\mathrm{d}\nu_{\rm SM}/\mathrm{d}x > 0$ when $x > x_c$. This is consistent with Fig. 6, which shows the curvature of the wells in the PES increasing with x when $x > x_c$. It is also consistent with CBEs reducing $|\Delta\mathcal{E}^{\rm att}|$ so that $\Delta\mathcal{E}$ is dominated by $\Delta\mathcal{E}^{\rm rep}$, and it is consistent with our simple ionic picture of bonding and energetics because the SM involves the relative motion of Ti and its O_6 cage and so their equilibrium relative displacement is sensitive to the strength of the Ti-O attraction.

The equilibrium structure can be specified in $\sqrt{\text{mass}}$-scaled Cartesian coordinates by the vector $\mathbf{U}^{\rm eq}(x) \equiv (\sqrt{m_{\rm Ba}}\, r^{\rm eq,x}_{\rm Ba}(x), \cdots, \sqrt{m_{\rm O}}\, r^{\rm eq,z}_{\rm O_3}(x))^{\rm T} \in \mathbb{R}^{15}$, where $\mathbf{r}^{\rm eq}_{\rm Y} \equiv (r^{\rm eq,x}_{\rm Y}, r^{\rm eq,y}_{\rm Y}, r^{\rm eq,z}_{\rm Y})^{\rm T}$. With the unit cell fixed ($\mathbf{h} = \mathbf{h}^{\rm eq}_0$), the normalized symmetry-breaking $\sqrt{\text{mass}}$-scaled displacement vector, $(\mathbf{U}^{\rm eq}(x) - \mathbf{U}^{\rm eq}(0))\,/|\mathbf{U}^{\rm eq}(x) - \mathbf{U}^{\rm eq}(0)|$, can be expressed exactly as a superposition of $\mathbf{\Gamma}$-point A_1 optic mode eigenvectors of the photoexcited R3m crystal. Therefore, its squared projections onto the LM, SM, and AM eigenvectors should sum to one and be in proportion to the squared amplitudes of the $\mathbf{\Gamma}$-point phonons that would be excited via DECP at low T. At $x = 0.05$ e^-/ f.u. [0.12 e^-/ f.u.] we calculate them to be 0.04 [0.00], 0.94 [1.00], and 0.01 [0.00], respectively. This substantiates our claim that the SM could *selectively* be excited via DECP.

Note that, because the FM and the CM share the same eigenvector, displacive excitation of the FM would also excite the CM to some degree. Therefore pump-probe spectroscopy could be used to further explore the intimate relationship between these modes and to confirm, or correct, the picture proposed by Hlinka *et al.* [48].

E. Electron doped $BaTiO_3$

Electron-doped BTO, including $La_yBa_{1-y}TiO_3$, $BaNb_yTi_{1-y}O_3$, and $BaTiO_{3-y/2}$, has been studied extensively [17–20, 44, 98–100, 123–127], with particular recent interest in disputed [20] reports that ferroelectricity can coexist with metallic conductivity. However, despite broad agreement on *what* effects $n-$doping has on BTO's structure, transition temperatures, and phonon frequencies, experiments do not agree quantitatively on the doping densities or carrier densities at which these effects occur [17–19]. In this section we use our simple assumptions about bonding and energetics to explain many of the observed properties of doped BTO and, in particular, its polar metallic phase.

It is common to try to understand dilutely $n-$doped BTO by relating its properties and behaviour to those of a pure BTO crystal to which CBEs and compensating positive charges have been added. However, as discussed in Sec. I D and Sec. III B, given the total density, y, of electrons added to a sample by doping, it is very difficult to determine the appropriate density, $x(y)$, of CBEs in pure BTO to compare the sample to. This is because an unknown fraction, $1 - x(y)/y$, of the y extra electrons per unit volume remain bound to the impurities and vacancies that introduce them to the crystal. Electrons bound to dopants should not be counted as CBEs because, instead of occupying the CB of their host crystal, they remain in localized donor states below the CB.

The *free* electron density, $z(y)$, measured from the Hall effect is also expected to differ from $x(y)$ because it only counts electrons whose attraction to ion cores is weaker than the Lorentz force from the applied magnetic field. It is clear from Fig. 8 that the rates of change of $q_{\rm Ti}$ and $3\times q_{\rm O}$ with respect to x have opposite signs and almost equal magnitudes, whereas the number of interstitial electrons in each unit cell increases relatively slowly with x. This implies that most CBEs remain in and around the Ti-O bond. As discussed in Sec. I C 3, local fields tend to be much stronger than long-range fields, making it highly unlikely that all of these 'bound' CBEs would be stripped away from Ti and O ions in a Hall measurement. The interstitial electrons, on the other hand, are more delocalized because they feel a weaker attraction to ion cores and are likely to make the greatest con-

tribution to $z(y)$. Whether or not $z(y)$ can be interpreted as a rough estimate of the density of *interstitial* CBEs, it is almost certainly the case that $z(y)/x(y) \ll 1$. Therefore measured carrier densities are not directly comparable to the densities of CBEs in calculations such as ours. However, in the dilute doping limit ($y \to 0$) the average number of electrons bound to each dopant or vacancy is independent of y, which implies that $x \propto y$. If the Hall density is proportional to the interstitial electron density, the linearity evident in Fig. 8 implies that $z \propto x \propto y$.

The potential energy as a function of the positions of all nuclei in the crystal, which we refer to as the 'full' PES, is significantly altered when the CB is populated by electrons. This is clear from the dependence of the 'reduced' PES, plotted in Fig. 6, on x. If these changes are caused by a weakening of the Ti-O attraction, as our assumptions about bonding and energetics imply, CBEs would also lower the barriers to reversal of polarity on each primitive cell's 'local' PES ($\Delta\mathcal{E}^{\mathrm{SM+CM}}$ in the simplistic model of Sec. I B) and the barrier to switching the polarization of a ferroelectric domain. Therefore we expect CBEs to reduce both T_C and E_c. Several experimental works [17–19, 44], have shown that $n-$doping reduces T_C and a downward shift of the P4mm $\to$ Amm2 transition temperature has also been observed [18, 19, 124]. Furthermore, although all three FE phases have been observed in doped BTO, the magnitudes of the polar distortions are found to be remarkably reduced [17]. This is also consistent with our physical model and the calculations presented in Fig. 6.

By reducing the degree to which polar distortions of individual cells are aligned, thermal disorder reduces the potential energy gained from these distortions [49]. Therefore, at fixed T, the CBE-induced change in each cell's local PES is qualitatively similar to the T-induced change in the *time average* of each local PES at fixed x [49]. Both are qualitatively similar to the curves plotted in Fig. 6: As x or T increases, the double well becomes shallower, the energy barrier to reversal of polarity is lowered and, when x or T are high enough, there is only a single well of increasing curvature. The increase in curvature with x when $x > x_c$ (Fig. 6), and with T when $T > T_C$, are both consistent with an increasing dominance of $\Delta\mathcal{E}^{\mathrm{rep}}$ over $\Delta\mathcal{E}^{\mathrm{att}}$, caused by the weakening of $\Delta\mathcal{E}^{\mathrm{att}}$. The quadratic contribution to $\Delta\mathcal{E}(\delta_{\mathrm{Ti}})$ in Eq. 3 vanishes at $x = x_c$ because $(\Delta\mathcal{E}^{\mathrm{att}})''(0) = -(\Delta\mathcal{E}^{\mathrm{rep}})''(0)$. When $x > x_c$ the coefficient of this quadratic term is positive because the negative contribution to it from $\Delta\mathcal{E}^{\mathrm{att}}$ has reduced in magnitude. As either x increases above x_c or T increases above T_C, the curvature should continue to increase because CBEs and thermal disorder both continue to reduce the magnitude of $\Delta\mathcal{E}^{\mathrm{att}}$. As a result, the SM of the Pm$\bar{3}$m phase, which incorporates the remnants of the FE phase's CM and FM, is expected to harden and become less harmonic with increasing x or T. The hardening of Pm$\bar{3}$m's SM with increasing T is observed experimentally [31, 46, 48], but we are not aware of any measurements of the Pm$\bar{3}$m SM frequency at multiple carrier densities and the same temperature.

In a FE crystal the shallowing of the double well as x or T increases reduces each well's curvature and lowers the energy barrier separating them. The reduction in depth and curvature reduces the FM frequency and makes it more anharmonic, while the lowering of the energy barrier activates the CM. In the simplistic model of Sec. I B, the CM emerges because the magnitude of the Boltzmann factor's exponent, $\Delta\mathcal{E}^{\mathrm{SM+CM}}/k_BT$, is reduced, which increases the probability of hopping between the two energy basins. Therefore, in FE phases we should expect an increase in x or T to cause the FM spectral peak to soften, to broaden, to lower in intensity, and to develop a low frequency tail. The CM is responsible for the tail and for the reduction in spectral intensity of the FM: referring again to Sec. I B, this is because each local mode can either oscillate about one of its local energy minima or hop between energy basins, but it can't do both simultaneously. Hwang *et al.* observed precisely these features in optical conductivity spectra [44]. They contrasted $\mathrm{d}\nu_{\mathrm{SM}}/\mathrm{d}x < 0$ in BTO with literature reports that $\mathrm{d}\nu_{\mathrm{SM}}/\mathrm{d}x > 0$ in doped $SrTiO_3$ [128, 129]. As shown in Fig. 6, the FE instability is critically weakened at $x = x_c$ and, like undoped STO, for which $x_c = 0$, BTO is an incipient ferroelectric. Our finding that $\mathrm{d}\nu_{\mathrm{SM}}/\mathrm{d}x > 0$ when $x > x_c$, due to the increasing dominance of $\Delta\mathcal{E}^{\mathrm{rep}}$ over $\Delta\mathcal{E}^{\mathrm{att}}$, appears to explain the different behaviours of BTO and STO at low values of x.

Our results imply that polar metals can exist if enough delocalized interstitial CBEs for metallic conductivity are created before the Ti-O attraction responsible for local polar distortions is critically weakened by CBEs that are bound to atoms. Although delocalized electrons would not screen the Ti-O attraction that causes local polar distortions effectively, the long range ordering of these polar distortions would be vulnerable to screening by them. This is consistent with the work of Fujioka *et al.* [18], who found that metallic BTO had reduced polarization anisotropy, and enhanced SM spectral intensity. The former is evidence of reduced long-range order and suggests the existence of a nanoscale complex domain structure. The latter is consistent with the ions' polarizabilities increasing and further supports our contention that the short-range Ti-O attraction is responsible for the FE instability.

One obvious difference between photoexcited BTO and $n-$doped BTO is that in the latter dopant defects perturb the lattice, which helps to reduce $|\mathbf{P}|$ by weakening long range order. Disorder also softens the SM [44] by reducing the depths of the double wells in the PES. In the simplistic model of Sec. I B, disorder among neighbouring cells can strongly influence the $\mathbf{d} - \mathbf{d}$ coupling term, which is responsible for the $\mathbf{d} \parallel \mathbf{P}$ well in each local PES being deeper, on average, than the $\mathbf{d} \parallel -\mathbf{P}$ well. Disorder lessens this asymmetry, thereby reducing the degree of alignment of cells' polarities, lowering the energy barriers to polarity reversal, and reducing the average

magnitudes of their polar distortions. In FE phases this would soften the FM and increase the spectral intensity of the CM at the expense of the FM. Although all of this suggests that vacancies and dopants have a deleterious effect on polar order, it has been suggested that the more delocalised and itinerant CBEs that are present in polar metallic BTO help to screen perturbations of the lattice by defects and impurities, thereby helping to stabilise the FE phases in metallic BTO [17].

Another difference between photoexcited and electron-doped BTO is that photoexcitation creates *two* populations of carriers: CBEs and VBHs. In the Hall measurements performed by Kolodiazhnyi [124] and Fujioka *et al.* [18] it was found that the Hall coefficients (R_H) of all semiconducting and metallic doped samples were negative and rather insensitive to T above the temperature range of stability of the R3m phase. However, both groups found that R_H, which is negative at most temperatures, changes rapidly as T is reduced in the R3m phase. Its most interesting and puzzling behaviour was observed in metallic samples: R_H becomes much less negative as T is reduced and even changes sign below $\sim 50-100$ K, indicating that holes become the dominant charge carrier in the $T \to 0$ limit [18, 124]. We do not add to the explanation offered by Kolodiazhnyi for the low-T $p-$type conduction, but we can offer an explanation for the dramatic reduction of $|R_H|$ as a conducting sample is cooled. In the work of Fujioka *et al.* a correlation is apparent between the temperature dependences of R_H and the IR spectral intensity of the FM. If we were correct, above and in Sec. I B, to attribute the reduction of the FM spectral intensity as T increases to the emergence of the CM, Fujioka's data shows that $|R_H|$ increases as the CM becomes more active. This is not surprising because, as explained in Sec. I B, the CM involves each cell hopping between multiple polar states. In R3m this means that Ti moves further away from the three closest O ions to it, thereby weakening or breaking three Ti-O bonds, and moves closer to the other three nearby O ions, thereby strengthening those bonds. This breaking and reforming of bonds means that, on average, bonds are weaker. The structural disorder when the CM is active further weakens bonds by reducing $|\Delta\mathcal{E}^{\rm att}|$. We have argued above that most of the CBEs that are bound to Ti and O would not have the freedom to respond to long range fields. It follows that the proportion CBEs capable of contributing to a Hall measurement should increase when bonds are weaker. This may explain why R_H becomes less negative as the temperature is lowered: fewer electrons are mobile because their net attraction to ions is stronger on average.

We have suggested that ultrashort laser pulses could be used in optoelectronic devices to facilitate FE domain switching by lowering T_C and E_c. However, a $> E_g$ laser pulse that creates a critical density (x_c) of CBEs would heat the crystal by ~ 300 K, assuming that no photon emission occurs. One way to avoid this would be to use *both* doping and photoexcitation to generate carriers. Doping reduces E_g, thereby moderately lowering the heat generated per photon absorbed, and it reduces the number of CBEs that must be generated by photoexcitation to lower E_c to the desired level. This would substantially reduce the amount of heat generated in the device. It might be possible to achieve a further reduction if, instead of exciting VBEs into the CB, the electrons occupying donor states just below the CB could be excited into the CB. Furthermore, as mentioned at the beginning, BTO is a prototype ferroelectric perovskite which shares many of its properties with other similar materials. This increases the probability that, in one such material, a combination of doping and photoexcitation could be used to improve the speed and efficiency of ferroelectric devices.

IV. CONCLUSION

We have calculated the effects of CBEs on the soft mode and ferroelectricity in BTO. Our objective has been to demonstrate that the structure, polarization, and phonon dynamics of BTO can be controlled by tuning the CBE density, and to explain, in simple terms, the mechanisms by which they influence these properties.

We have suggested several ways to exploit the sensitivity of ferroelectricity to the CBE density. One of these is to facilitate ferroelectric domain switching, either by using laser pulses to lower E_c temporarily or by adding $n-$dopants to reduce it permanently. Another is to use ultrafast pump-probe spectroscopy to selectively excite the FM and CM and to monitor their decay into other modes. It is hoped that a great deal, of fundamental importance to the physics of ferroelectrics, might be learned by studying these modes at low T as they thermalize by coupling with other excitations. Our calculations also suggest that CBEs lower T_C and could even be used to induce a purely-displacive transition to the $Pm\bar{3}m$ PE structure at low T.

Our work is based on two premises, which differ from the assumptions on which some other studies of ferroelectricity in perovskites are based. They are that BTO's bonding is best described as ionic and that its ferroelectric phases are stabilized, not by long range Coulomb interactions, but by the attraction between neighbouring Ti and O ions. The idea that the ferroelectric instability is caused by short-range forces appears to explain all of BTO's properties, whereas the idea that long-range Coulomb interactions are required seems incompatible with the existence of a polar metallic phase. We find that assuming ionicity and that the attraction between neighbouring ions stabilizes the **P** field allows us to suggest simple and intuitive explanations for many of the experimentally-observed properties of both pure and electron-doped BTO, including its polar metallic phase. We also find perfect consistency between these assumptions and the results of our DFT calculation.

[1] A. Feteira, D. C. Sinclair, I. M. Reaney, Y. Somiya, and M. T. Lanagan, J. Am. Ceram. Soc. **87**, 1082 (2004).
[2] H. Jaffe, Ind. Eng. Chem. Res. **42**, 264 (1950).
[3] M. Acosta, N. Novak, V. Rojas, S. Patel, R. Vaish, J. Koruza, G. A. Rossetti, and J. Rödel, Appl. Phys. Rev. **4**, 41305 (2017).
[4] V. S. Dharmadhikari and W. W. Grannemann, J. Appl. Phys. **53**, 8988 (1982).
[5] S. Fahy and R. Merlin, Phys. Rev. Lett. **73**, 1122 (1994).
[6] A. Zenkevich, Y. Matveyev, K. Maksimova, R. Gaynutdinov, A. Tolstikhina, and V. Fridkin, Phys. Rev. B **90**, 161409 (2014).
[7] Z. Xiao, Y. Yuan, Y. Shao, Q. Wang, Q. Dong, C. Bi, P. Sharma, A. Gruverman, and J. Huang, Nat. Mater. **14**, 193 (2015).
[8] S. Wang, X. Liu, L. Li, C. Ji, Z. Sun, Z. Wu, M. Hong, and J. Luo, J. Am. Chem. Soc. **141**, 7693 (2019).
[9] V. M. Fridkin, Ferroelectrics **484**, 1 (2015).
[10] A. Rosa, D. Tulli, P. Castera, A. M. Gutierrez, A. Griol, M. Baquero, B. Vilquin, F. Eltes, S. Abel, J. Fompeyrine, and P. Sanchis, Opt. Mater. Express **7**, 4328 (2017).
[11] Z. Shen, X. Wang, B. Luo, and L. Li, J. Mater. Chem. A **3**, 18146 (2015).
[12] J. Li, J. Claude, L. E. Norena-Franco, S. I. Seok, and Q. Wang, Chem. Mater **20**, 6304 (2008).
[13] Y. Yang, H. Wang, L. Bi, Q. Zheng, G. Fan, W. Jie, and D. Lin, J. Eur. Ceram. Soc. **39**, 3051 (2019).
[14] Y. Lin, D. Li, M. Zhang, S. Zhan, Y. Yang, H. Yang, and Q. Yuan, ACS Appl. Mater. Interfaces **11**, 36824 (2019).
[15] M. Cardona, Phys. Rev. **140**, A651 (1965).
[16] K. Suzuki and K. Kijima, Jpn. J. Appl. Phys. **44**, 2081 (2005).
[17] T. Kolodiazhnyi, M. Tachibana, H. Kawaji, J. Hwang, and E. Takayama-Muromachi, Phys. Rev. Lett. **104**, 147602 (2010).
[18] J. Fujioka, A. Doi, D. Okuyama, D. Morikawa, T. Arima, K. N. Okada, Y. Kaneko, T. Fukuda, H. Uchiyama, D. Ishikawa, A. Q. R. Baron, K. Kato, M. Takata, and Y. Tokura, Sci. Rep. **5**, 13207 (2015).
[19] F. Cordero, F. Trequattrini, F. Craciun, H. T. Langhammer, D. A. B. Quiroga, and P. S. Silva, Phys. Rev. B **99**, 064106 (2019).
[20] I.-K. Jeong, S. Lee, S.-Y. Jeong, C. J. Won, N. Hur, and A. Llobet, Phys. Rev. B **84**, 064125 (2011).
[21] J. M. Pérez-mato, S. Ivantchev, A. García, and I. Etxebarria, Ferroelectrics **236**, 93 (2000).
[22] J. F. Scott, Rev. Mod. Phys. **46**, 83 (1974).
[23] H. F. Kay and P. Vousden, London, Edinburgh Dublin Philos. Mag. J. Sci. **40**, 1019 (1949).
[24] G. H. Kwei, A. C. Lawson, S. J. L. Billinge, and S. W. Cheong, J. Phys. Chem. **97**, 2368 (1993).
[25] B. Ravel, E. A. Stern, R. I. Vedrinskii, and V. Kraizman, Ferroelectrics **206**, 407 (1998).
[26] B. Zalar, V. V. Laguta, and R. Blinc, Phys. Rev. Lett. **90**, 037601 (2003).
[27] E. A. Stern and Y. Yacoby, J Phys Chem Solids **57**, 1449 (1996).
[28] M. S. Senn, D. A. Keen, T. C. A. Lucas, J. A. Hriljac, and A. L. Goodwin, Phys. Rev. Lett. **116**, 207602 (2016).
[29] Y. Qi, S. Liu, I. Grinberg, and A. M. Rappe, Phys. Rev. B **94**, 134308 (2016).
[30] J. Petzelt, G. V. Kozlov, and A. A. Volkov, Ferroelectrics **73**, 101 (1987).
[31] J. Petzelt, Ferroelectrics **375**, 156 (2008).
[32] M. W. Wefers, H. Kawashima, and K. A. Nelson, J. Phys. Chem. Sol. **57**, 1425 (1996).
[33] K. Istomin, V. Kotaidis, A. Plech, and Q. Kong, Appl. Phys. Lett. **90**, 022905 (2007).
[34] F. Rubio-Marcos, A. Del Campo, P. Marchet, and J. F. Fernández, Nat. Comm. **6**, 6594 (2015).
[35] H. Akamatsu, Y. Yuan, V. A. Stoica, G. Stone, T. Yang, Z. Hong, S. Lei, Y. Zhu, R. C. Haislmaier, J. W. Freeland, L.-Q. Chen, H. Wen, and V. Gopalan, Phys. Rev. Lett. **120**, 096101 (2018).
[36] F. Rubio-Marcos, D. A. Ochoa, A. Del Campo, M. A. Garcia, G. R. Castro, J. F. Fernandez, and J. E. Garcia, Nat. Phot. **12**, 29 (2018).
[37] D. Paez-Margarit, F. Rubio-Marcos, D. A. Ochoa, A. Del Campo, J. F. Fernandez, and J. E. Garcia, ACS Appl. Mater. Interfaces **10**, 21804 (2018).
[38] T. Li, A. Lipatov, H. Lu, H. Lee, J.-W. Lee, E. Torun, L. Wirtz, C.-B. Eom, J. Iniguez, A. Sinitskii, and A. Gruverman, Nat. Comm. **9** (2018).
[39] T. Qi, Y. H. Shin, K. L. Yeh, K. A. Nelson, and A. M. Rappe, Phys. Rev. Lett. **102**, 247603 (2009).
[40] F. Chen, Y. Zhu, S. Liu, Y. Qi, H. Y. Hwang, N. C. Brandt, J. Lu, F. Quirin, H. Enquist, P. Zalden, T. Hu, J. Goodfellow, M. J. Sher, M. C. Hoffmann, D. Zhu, H. Lemke, J. Glownia, M. Chollet, A. R. Damodaran, J. Park, Z. Cai, I. W. Jung, M. J. Highland, D. A. Walko, J. W. Freeland, P. G. Evans, A. Vailionis, J. Larsson, K. A. Nelson, A. M. Rappe, K. Sokolowski-Tinten, L. W. Martin, H. Wen, and A. M. Lindenberg, Phys. Rev. B **94**, 180104 (2016).
[41] A. Subedi, Phys. Rev. B **92**, 214303 (2015).
[42] R. Mankowsky, A. von Hoegen, M. Först, and A. Cavalleri, Phys. Rev. Lett. **118**, 197601 (2017).
[43] A. Cavalleri, S. Wall, C. Simpson, E. Statz, D. W. Ward, K. A. Nelson, M. Rini, and R. W. Schoenlein, Nature **442**, 664 (2006).
[44] J. Hwang, T. Kolodiazhnyi, J. Yang, and M. Couillard, Phys. Rev. B **82**, 214109 (2010).
[45] R. E. Cohen, Nature **358**, 136 (1992).
[46] Y. Luspin, J. L. Servoin, and F. Gervais, J. Phys. C: Solid State Phys. **13**, 3761 (1980).
[47] Y. Girshberg and Y. Yacoby, Solid State Commun. **103**, 425 (1997).
[48] J. Hlinka, T. Ostapchuk, D. Nuzhnyy, J. Petzelt, P. Kuzel, C. Kadlec, P. Vanek, I. Ponomareva, and L. Bellaiche, Phys. Rev. Lett. **101**, 167402 (2008).
[49] J. Fallon, *Multiscale theory and simulation of barium titanate*, Ph.D. thesis, Imperial College London (2014).
[50] M. Christensen, A. B. Abrahamsen, N. B. Christensen, F. Juranyi, N. H. Andersen, K. Lefmann, J. Andreasson, C. R. H. Bahl, and B. B. Iversen, Nat. Mater. **7**, 811 (2008).
[51] R. E. Cohen and H. Krakauer, Phys. Rev. B **42**, 6416 (1990).
[52] W. Zhong, D. Vanderbilt, and K. M. Rabe, Phys. Rev.

B **52**, 6301 (1995).
[53] M. Lines and A. Glass, *Principles and Applications of Ferroelectrics and Related Materials*, International series of monographs on physics (OUP Oxford, 2001).
[54] R. Resta, Model. Simul. Mater. Sci. Eng **11**, R69 (2003).
[55] H. J. Zhao, A. Filippetti, C. Escorihuela-Sayalero, P. Delugas, E. Canadell, L. Bellaiche, V. Fiorentini, and J. Íñiguez, Phys. Rev. B **97**, 054107 (2018).
[56] P. Tangney and S. Scandolo, J. Chem. Phys. **117**, 8898 (2002).
[57] P. Tangney and S. Scandolo, J. Chem. Phys. **119**, 9673 (2003).
[58] J. R. Kermode, S. Cereda, P. Tangney, and A. De Vita, J. Chem. Phys. **133**, 094102 (2010).
[59] X. J. Han, L. Bergqvist, P. H. Dederichs, H. Mueller-Krumbhaar, J. K. Christie, S. Scandolo, and P. Tangney, Phys. Rev. B **81**, 134108 (2010).
[60] J. Sarsam, M. W. Finnis, and P. Tangney, J. Chem. Phys. **139**, 204704 (2013).
[61] V. Nemytov, *Towards an accurate and transferable charge transfer model in polarisable interatomic potentials*, Ph.D. thesis, Imperial College London (2019).
[62] P. Karen, P. McArdle, and J. Takats, Pure Appl. Chem. **88**, 831 (2016).
[63] L. Pauling, C. University, and C. U. Press, *The Nature of the Chemical Bond and the Structure of Molecules and Crystals: An Introduction to Modern Structural Chemistry*, George Fisher Baker Non-Resident Lecture Series (Cornell University Press, 1960).
[64] C. H. L. Goodman, Nature **187**, 590 (1960).
[65] E. Mooser and W. B. Pearson, Nature **190**, 406 (1961).
[66] W. Cochran, Nature **191**, 60 (1961).
[67] J. C. PHILLIPS, Rev. Mod. Phys. **42**, 317 (1970).
[68] D. R. Jennison and A. B. Kunz, Physical review B **13**, 5597 (1976).
[69] P. A. Madden and M. Wilson, Chem. Soc. Rev. **25**, 339 (1996).
[70] G. B. Bacskay, J. R. Reimers, and S. Nordholm, Journal of Chemical Education **74**, 1494 (1997), https://doi.org/10.1021/ed074p1494.
[71] M. Jansen and U. Wedig, Angewandte Chemie International Edition **47**, 10026 (2008), https://onlinelibrary.wiley.com/doi/pdf/10.1002/anie.200803605.
[72] A. Walsh, A. A. Sokol, J. Buckeridge, D. O. Scanlon, and C. R. A. Catlow, The Journal of Physical Chemistry Letters **8**, 2074 (2017), pMID: 28468501, https://doi.org/10.1021/acs.jpclett.7b00809.
[73] A. Walsh, A. A. Sokol, J. Buckeridge, D. O. Scanlon, and C. R. A. Catlow, Nature Materials **17**, 958 (2018).
[74] D. A. McQuarrie, P. A. Rock, and E. B. Gallogly, *General Chemistry* (The Royal Society of Chemistry, 2011).
[75] R. Ouellette and J. Rawn, *Principles of Organic Chemistry* (Elsevier Science, 2015).
[76] U. Zürcher, *Electrostatics at the Molecular Level* (IOP Concise Physics and Morgan & Claypool Publishers, 2018).
[77] G. N. Lewis, Journal of the American Chemical Society **38**, 762 (1916), https://doi.org/10.1021/ja02261a002.
[78] R. J. Gillespie and E. A. Robinson, Journal of Computational Chemistry **28**, 87 (2007), https://onlinelibrary.wiley.com/doi/pdf/10.1002/jcc.20545.
[79] R. van Leeuwen (Academic Press, 2003) pp. 25 – 94.
[80] W. Kohn and L. J. Sham, Phys. Rev. **140**, A1133 (1965).
[81] P. Hohenberg and W. Kohn, Phys. Rev. **136**, B864 (1964).
[82] J. L. Bao, P. Verma, and D. G. Truhlar, Phys. Chem. Chem. Phys. **20**, 23072 (2018).
[83] A. G. Kvashnin, D. G. Kvashnin, and A. R. Oganov, Scientific Reports **9**, 14267 (2019).
[84] B. Li, A. Michaelides, and M. Scheffler, Phys. Rev. B **76**, 075401 (2007).
[85] A. J. Rowley, P. Jemmer, M. Wilson, and P. A. Madden, The Journal of Chemical Physics **108**, 10209 (1998).
[86] J. Sarsam, *Development and application of atomistic force fields for ionic materials*, Ph.D. thesis, Imperial College London (2013).
[87] D. G. Pettifor and I. I. Oleinik, Phys. Rev. B **59**, 8487 (1999).
[88] M. Wilson, P. A. Madden, M. Hemmati, and C. A. Angell, Phys. Rev. Lett. **77**, 4023 (1996).
[89] R. E. Cohen, Nature **362**, 213 (1993).
[90] M. Posternak, R. Resta, and A. Baldereschi, Phys. Rev. B **50**, 8911 (1994).
[91] R. E. Cohen and H. Krakauer, Ferroelectrics **136**, 65 (1992).
[92] R. E. Cohen, L. L. Boyer, and M. J. Mehl, Phys. Rev. B **35**, 5749 (1987).
[93] C. Pinilla, M. Acuña-Rojas, N. Seriani, and S. Scandolo, Computational Materials Science **126**, 351 (2017).
[94] Y. Wang, X. Liu, J. D. Burton, S. S. Jaswal, and E. Y. Tsymbal, Phys. Rev. Lett. **109**, 247601 (2012).
[95] M. S. Senn, D. A. Keen, T. C. A. Lucas, J. A. Hriljac, and A. L. Goodwin, Phys. Rev. Lett. **116**, 207602 (2016).
[96] P. H. Fang and W. S. Brower, Phys. Rev. **113**, 456 (1959).
[97] C. Neusel and G. A. Schneider, J Mech Phys Solids **63**, 201 (2014).
[98] K. Härdtl and R. Wernicke, Solid State Commun. **10**, 153 (1972).
[99] K. Page, T. Kolodiazhnyi, T. Proffen, A. K. Cheetham, and R. Seshadri, Phys. Rev. Lett. **101**, 205502 (2008).
[100] T. Kolodiazhnyi, A. Petric, M. Niewczas, C. Bridges, A. Safa-Sefat, and J. E. Greedan, Phys. Rev. B **68**, 085205 (2003).
[101] M. Choi, F. Oba, and I. Tanaka, Appl. Phys. Lett. **98**, 172901 (2011).
[102] N. Tsunoda, Y. Kumagai, and F. Oba, Phys. Rev. Materials **3**, 114602 (2019).
[103] S. K. Sundaram and E. Mazur, Nat. Mater. **1**, 217 (2002).
[104] J. M. Richter, F. Branchi, F. Valduga de Almeida Camargo, B. Zhao, R. H. Friend, G. Cerullo, and F. Deschler, Nat. Comm. **8**, 376 (2017).
[105] H. Wen, P. Chen, M. P. Cosgriff, D. A. Walko, J. H. Lee, C. Adamo, R. D. Schaller, J. F. Ihlefeld, E. M. Dufresne, D. G. Schlom, P. G. Evans, J. W. Freeland, and Y. Li, Phys. Rev. Lett. **110**, 037601 (2013).
[106] H. J. Zeiger, J. Vidal, T. K. Cheng, E. P. Ippen, G. Dresselhaus, and M. S. Dresselhaus, Phys. Rev. B **45**, 768 (1992).
[107] K. Ishioka and O. V. Misochko, "Coherent lattice oscillations in solids and their optical control," in *Progress in Ultrafast Intense Laser Science: Volume V* (Springer Berlin Heidelberg, Berlin, Heidelberg, 2010) pp. 23–46.
[108] J. Weerasinghe, L. Bellaiche, T. Ostapchuk, P. Kužel,

C. Kadlec, S. Lisenkov, I. Ponomareva, and J. Hlinka, MRS Commun **3**, 41–45 (2013).
[109] P. Tangney and S. Fahy, Phys. Rev. Lett. **82**, 4340 (1999).
[110] P. Tangney and S. Fahy, Phys. Rev. B **65**, 054302 (2002).
[111] E. D. Murray, D. M. Fritz, J. K. Wahlstrand, S. Fahy, and D. A. Reis, Phys. Rev. B **72**, 060301 (2005).
[112] S. Sanna, C. Thierfelder, S. Wippermann, T. P. Sinha, and W. G. Schmidt, Phys. Rev. B **83**, 054112 (2011).
[113] E. Najafi, V. Ivanov, A. Zewail, and M. Bernardi, Nat. Commun. **8**, 15177 (2017).
[114] X. Gonze, B. Amadon, P. M. Anglade, J. M. Beuken, F. Bottin, P. Boulanger, F. Bruneval, D. Caliste, R. Caracas, M. Côté, T. Deutsch, L. Genovese, P. Ghosez, M. Giantomassi, S. Goedecker, D. Hamann, P. Hermet, F. Jollet, G. Jomard, S. Leroux, M. Mancini, S. Mazevet, M. Oliveira, G. Onida, Y. Pouillon, T. Rangel, G.-M. Rignanese, D. Sangalli, R. Shaltaf, M. Torrent, M. Verstraete, G. Zerah, and J. Zwanziger, Comp. Phys. Comm. **180**, 2582 (2009).
[115] M. Torrent, F. Jollet, F. Bottin, G. Zérah, and X. Gonze, Comp. Mat. Sci. **42**, 337 (2008).
[116] P. E. Blöchl, Phys. Rev. B **50**, 17953 (1994).
[117] J. P. Perdew, A. Ruzsinszky, G. I. Csonka, O. A. Vydrov, G. E. Scuseria, L. A. Constantin, X. Zhou, and K. Burke, Phys. Rev. Lett. **100**, 136406 (2008).
[118] A. Togo and I. Tanaka, Scr. Mater. **108**, 1 (2015).
[119] W. Zhong, R. D. King-Smith, and D. Vanderbilt, Phys. Rev. Lett. **72**, 3618 (1994).
[120] P. Ghosez, X. Gonze, and J. P. Michenaud, Ferroelectrics **220**, 1 (1999).
[121] S. F. Yuk, K. C. Pitike, S. M. Nakhmanson, M. Eisenbach, Y. W. Li, and V. R. Cooper, Sci. Rep. **7**, 43482 (2017).
[122] Y. Iwazaki, T. Suzuki, Y. Mizuno, and S. Tsuneyuki, Phys. Rev. B **86**, 214103 (2012).
[123] T. Zhao, Z. H. Chen, F. Chen, H. B. Lu, G. Z. Yang, and H. S. Cheng, Appl. Phys. Lett. **77**, 4338 (2000).
[124] T. Kolodiazhnyi, Phys. Rev. B **78**, 045107 (2008).
[125] K. S. Takahashi, Y. Matsubara, M. S. Bahramy, N. Ogawa, D. Hashizume, Y. Tokura, and M. Kawasaki, Sci. Rep. **7**, 4631 (2017).
[126] X. Jing, W. Xu, C. Yang, J. Feng, A. Zhang, Y. Zeng, M. Qin, M. Zeng, Z. Fan, X. Gao, Jinwei a nd Gao, G. Zhou, X. Lu, and J. Liu, App. Phys. Lett. **110**, 182903 (2017).
[127] A. Sagdeo, A. Nagwanshi, P. Pokhriyal, A. K. Sinha, P. Rajput, V. Mishra, and P. R. Sagdeo, J. Appl. Phys. **123**, 161424 (2018).
[128] D. Bauerle, D. Wagner, M. Wohlecke, B. Dorner, and H. Kraxenberger, Zeitschrift Fur Physik B-Condensed Matter **38**, 335 (1980).
[129] D. Wagner, D. Bauerle, F. Schwabl, M. Wohlecke, B. Dorner, and H. Kraxenberger, Ferroelectrics **26**, 725 (1980).